View metadata, citation and similar papers at core.ac.uk
brought to you by CORE
provided by NASA Technical Reports Server

3 1176 00167 3079

NASA Contractor Report 165741

FOR REFERENCE

NOT TO BE TAKEN FROM THIS ROOM

VERIFICATION OF REFLECTANCE MODELS IN TURBID WATERS

FRED J. TANIS and DAVID R. LYZENGA

ENVIRONMENTAL RESEARCH INSTITUTE OF MICHIGAN
Ann Arbor, Michigan 48107

CONTRACT NASI-15512
APRIL 1981

NASA-CR-165741
19810024036

SEP

National Aeronautic and
Space Administration

Langley Research Center
Hampton, Virginia 23665

TABLE OF CONTENTS

N81-32579#

PREFACE

This final report as issued by the Applications Division of the Environmental Research Institute of Michigan (ERIM) under National Aeronautics and Space Administration (NASA) contract NAS1-15512 for the Langley Research Center (LaRC) covers the contract period from September 1, 1978 through April 15, 1981. The technical representative for the contract officer was Lamont R. Poole, Marine Environments Branch of LaRC with Dr. Charles Whitlock as alternate. The principal investigator was Fabian C. Polcyn, with important contributions to the technical program made by Fred J. Tanis and David R. Lyzenga. This research was conducted by the Applications Division under the direction of Mr. Donald S. Lowe.

This contract involves developing techniques to recognize various water pollutants from remotely sensed data. The approach required collection of aircraft multispectral scanner data together with data on the optical properties of selected pollutants.

Two joint LaRC/ERIM field experiments were conducted on the James River near Hopewell, Virginia. The first experiment was conducted between November 9-13, 1978 while the second test took place during the period from May 5, 1979 to June 6, 1979. Reporting of experimental data from these activities are included in LaRC technical reports under Technical Directives 1-129-29 and 1-129-32, as well as ERIM Technical Monthly Reports 137000-11-L through 18-L.

Five additional experiments were conducted by LaRC. The optical data from three of these experiments are reported in a LaRC publication [1]. It is the analysis of these five data sets which are the primary subject of this final report.

LIST OF FIGURES

LIST OF FIGURES (Continued)

LIST OF TABLES

PARTIAL LIST OF SYMBOLS

Symbol	Definition
a	absorption coefficient
b	scattering coefficient
B	backscatter fraction
c	extinction coefficient
n	index of refraction of water
$\beta(\theta)$	volume scattering function
θ	scattering angle, view angle
θ_o	solar zenith angle
ϕ	azimuth angle
ω_o	single-scattering albedo
μ	cosine of view angle
μ_o	cosine of solar zenith angle
μ_c	cosine of critical angle
$R(\theta,\phi,\theta',\phi')$	bi-directional reflectance function
$R(\mu, \mu_o)$	azimuthally averaged bi-directional reflectance function
R_H	hemispherical reflectance
L_W	total upwelling radiance below surface
$L_W^{\pm}$	total upwelling radiance above surface
L_D	upwelling radiance due to scattering of direct sunlight
L_S	upwelling radiance due to scattering of skylight
L_I	upwelling radiance due to scattering of internally reflected light
L	downwelling radiance below surface
E_D	direct solar irradiance below surface
E_S	diffuse (sky) irradiance below surface
$p(\mu)$	scattering phase function
$H(\mu)$	Chandrasekhar's H-function

1.0

INTRODUCTION

1.1 BACKGROUND

The primary source of sediment to the aquatic environment is freshwater runoff from non-point sources such as agricultural land, urban areas, and other land uses. Point discharges from municipal and industrial sources can also provide significant inputs of particulates. Interactions between sediment and chemical pollutants are complex but provide in general a significant transport mechanism for nutrients, trace metals and organic contaminants. Because particulates in water can strongly affect the quality of the aquatic environment the ability to monitor and predict source, transport, and fate has upmost importance to impact assessment and water quality management. Many estuarine processes and plume dynamics can be studied by tracing the distribution of suspended matter. Such studies require spatial and temporal resolutions not obtainable with standard oceanographic sampling methods.

In order to fully exploit the remote sensing capabilities for obtaining measurements of water parameters in estuarine and coastal waters we must understand the quantitative relationships between the observed optical properties and the inherent properties which are determined by concentrations of the various constituents.

The direct measurement either by in situ or in vitro techniques of the inherent optical properties is recognized as a difficult task requiring very sophisticated instrumentation [2,3]. The primary incentive in collecting these data is to utilize them in existing water optical models in order to predict the behavior of light in a water medium of suspended particles. Understanding the radiative transfer process in turbid water will allow remote sensing systems to monitor important features in the coatal and inland waters. A number of reflectance models have been reported in the ocean optics literature, most notably those of Gordon [4,5], Jain and Miller [6], and Plass, Humphreys and Kattawar [7]. Each of these models is based upon a simplification to the radiative transfer equation or its solution. To date these models have been almost exclusively applied to data from clear ocean waters. Moreover, most of these studies have lacked a complete data set with which to verify model predictions. The present study may be unique in two respects; (1) the measurement data are from highly turbid waters, and (2) measurements have been systematically made to describe the inherent optical properties together with upwelling and downwelling radiation. The initial purpose of this work is to verify existing models under turbid conditions and develop new models specifically for turbid water environments. The extended objective is to develop techniques which can extract pollution related information from the observed color of the coastal and estuarine waters.

Inherent optical properties of a water medium which are needed to describe the radiative transfer process include absorption as measured by the absorption coefficient, a, the volume scattering function $\beta(\theta)$ and the beam attenuation, c. These parameters are interrelated according to:

$$c = a + b \text{ where } b = 2\pi \int_0^\pi \beta(\theta) \sin\theta \, d\theta \qquad (1)$$

Thus, a and b are the fractional partitions of the total losses from beam of parallel monochromatic light due to absorption and scattering.

An <u>in vitro</u> capability to measure c, a, and $\beta(\theta)$ in turbid waters has been developed at the NASA/Langley Research Center. These instruments permit the collection of a complete set of the inherent optical properties for highly turbid waters.

1.2 OPTICAL MEASUREMENTS

During 1979 a series of five individual measurement sets were gathered by LaRC. Test sites included two locations in the Appomatox River

(A1 and A2) near Hopewell, Virginia, the Back River waters (B) at Hampton, Virginia, the Satilla and Ogeechee Rivers (G1 and G2) in the Georgia coastal area. At each of these test sites the measurements were made of underwater optical parameters, sea surface spectral radiance, and water chemical and particulate composition. The Virginia tests were all from moderately turbid waters with suspended solid concentrations of 14.4 mg/ℓ, 18.6 mg/ℓ, and 22.8 mg/ℓ respectively for sites A1, A2, and B. The waters of the Satilla and Ogeechee are, on the other hand, less turbid at 10.0 and 7.0 mg/ℓ, total suspended solids but with a large dissolved organic carbon component giving these waters a reddish color. Specific test site conditions for all sites are contained in Table 1. Underwater optical properties as measured <u>in vitro</u> are shown in Table A1 and A2 of Appendix A and in Reference [1]. These data include the beam attenuation coefficient, the absorption coefficient, and the volume scattering function $\beta(\theta)$ at 50 nm intervals over the wavelength range 450-800 nm. Three separate instruments were used to measure these parameters, (1) a combination beam attenuation and small angle scattering meter (SASM, $\theta = 0.374, 0.751, 1.49°$) developed by LaRC and patterned after the Scripps Institute of Oceanography ALSCAT instrument; (2) a Brice Phoenix (BP) scattering meter modified to accommodate large angle measurements ($25° \leq \theta \leq 155°$); and (3) the Langley spectral absorption coefficient instrument (SPACI) [8]. All three instruments employed optical interference filters with identical spectral range (400-800 nm) and resolution (10 nm). Standard errors for these instruments are reported to be as follows: (1) for the SASM less than 5% α and less than 12% $\beta(\theta)$; (2) for the modified BP less than 20% $\beta(\theta)$; and (3) for the SPACI less than 10% a.

Surface measurements of upwelling, downwelling, and vertical sky radiance spectra were made by LaRC concurrent with water sampling using a Tektronix J20/7J20 rapid scan spectrometer ($\sigma < 5\%\ L$). The total downwelling in radiance was obtained by viewing a horizontal Lambertian 99% reflector coated with Eastman 6080 white reflectance paint. The apparent upwelling radiance measured over water includes the inherent

TABLE 1

TEST SITE CONDITIONS

Sample	A1	A2	B	G1	G2
Date	5/23/79	6/5/79	8/29/79	11/4/79	11/4/79
Solar Zenith Angle	18°	53°	35°	33°	41°
Sky Conditions	Broken	Clear	Clear	Clear	Clear
Chlorophyll *a* (μg/ℓ)	15	10	13	2.1	3.9
Volatile Suspended Solids (mg/ℓ)	4.3	3.9	8.9	1.4	1.0
Inorganic Suspended Solids (mg/ℓ)	10.1	14.7	13.9		
Total Suspended Solids (mg/ℓ)	14.4	18.6	22.8	10	7
Dissolved Organic Carbon (mg/ℓ)	<10	<10	<10	12.5	19.3
Particle Size Range (μ)	0.45-26	0.45-42	0.45-52		
Secchi Disk Depth	0.8	0.5	1.4	1.0	0.6

radiance reflected from below the surface plus the surface specular reflection of diffuse skylight. The specular component was estimated by multiplying the vertical sky radiance by the Fresnel reflection coefficient (approximately 0.02). The inherent component was computed by subtracting the specular component from the total vertical upwelling radiance measurement. Estimated values of direct irradiance, diffuse irradiance and the inherent upwelling radiance L_w are given for each of the five measurement sites in Table A2. These calculations are discussed and compared with model results in section 3.0.

1.3 SUMMARY OF CONCLUSIONS

The present work was designed as an initial step to apply water reflectance modeling theory to a turbid water environment. Verification of water radiance models is a critical step and must be completed before one can develop quantitative algorithms to study coastal processes. To date very few verification studies have been initiated. The fact that the present study found partial agreement between model results and measurement data warrants further investigation of model limitations and definition of systematic errors. Measurement technology for water inherent optical properties and generalized modeling theory for radiative transfer process is available. Research programs must be supported to utilize this technology to develop a body of knowledge on the optical properties of various coastal water types. Coincident studies are needed to develop specific constituent algorithms for turbid waters so that benefits from remote sensing applications can be confirmed.

THIS PAGE INTENSIONALLY LEFT BLANK

2.0

DESCRIPTION OF WATER RADIANCE MODELS

Selected models which simplify the radiative transfer equation were used to evaluate each of the optical data sets. These models included Gordon's quasi-single scattering (QSS) model, his power series (GPS) approximation to Monte Carlo solutions, an adapted form of Chandrasekhar's (AC) exact solution for isotropic scattering [9], and the Jain two stream (TS) model [6] which is equivalent to that of Plass, et al [7]. Each of these models used the backscatter fraction B estimated from the measured $\beta(\theta)$ and the single scattering albedo, ω_0, as determined by forming the ratio b/(a + b). A Monte Carlo (MC) code was developed to approximate an exact solution of the radiative transfer equation for turbid waters. Simulation is considered to provide a more precise solution since it utilizes all of the scattering measurement data and describes a more complex set of possible photon interactions.

Our simulation model was based upon one developed by Ghovanlou [10] but with several modifications made to improve the efficiency as discussed in the next section. The probability distribution functions used for the Monte Carlo simulations were obtained by smoothing and integrating the fourteen raw measured values for each scattering function. Cubic spline functions were fitted and normalized prior to integration such that

$$\hat{c} - \hat{a} = 2\pi \int_0^{\pi} \hat{\beta}(\theta) \sin\theta \, d\theta . \tag{2}$$

The difference between the measured value of $\hat{c}$ and the measured value of $\hat{a}$ is an estimate of the total scattering coefficient, which is made equal to the above integration so as to obtain a self-consistent data set. It is recognized that in this procedure we have ignored possible errors in c and a. However, our analysis has shown the above integration to be highly sensitive to the values of $\beta(\theta)$, especially for small θ. A decription of our analysis procedure and resulting modifications to $\beta(\theta)$ are contained in Appendix A.

Photons were selected from the resultant probability distribution by interpolation on twenty-five intervals of equal probability between 0 and 180°. In the simulation, photons emerging within the critical angle were recorded by scattering order and zenith angle.

2.1 MODEL CALCULATIONS

Each of these models was used as a means to calculate three distinct components of the upwelling radiance $L_W(\theta, \theta_0)$ just below the water surface.

$$L_W(\theta, \theta_0) = L_D(\theta,\theta_0) + L_S(\theta) + L_I(\theta) \qquad (3)$$

where $L_D(\theta,\theta_0)$ is due to scattering of direct sunlight
$L_S(\theta)$ is due to scattering of skylight
$L_I(\theta)$ is due to scattering of internally reflected light
θ and θ_0 are the view angle and solar zenith angle, respectively.

The contribution of internal reflection to turbid water reflectance can be significant.

In the following, the variables θ and θ_0 are replaced by their cosines, μ and μ_0, for convenience. Further, the dependence on the azimuthal angle ϕ is neglected for simplicity. Each of the three components can be calculated in terms of the reflectance function $R(\mu,\mu_0)$. The component $L_D(\mu,\mu_0)$ is obtained simply as $E_D \cdot R(\mu,\mu_0)$ where E_D is the direct solar irradiance just below the surface at θ_0. The skylight contribution on the other hand requires the integration:

$$L_S(\mu) = \int_0^{2\pi}\int_{\mu_c}^{1} R(\mu,\mu')L(\mu')\mu'd\mu'd\phi \qquad (4)$$

where $L(\mu')$ is the downwelling radiance distribution below the surface, and μ_c is the cosine of the critical angle, i.e., $\mu_c = \sqrt{1-n^{-2}}$ and n is the index of refraction of water.

If it is assumed that the downward sky radiance is uniform within the cone defined by the critical angle then (4) becomes

$$L_S(\mu) = 2n^2 E_S \int_{\mu_c}^{1} R(\mu,\mu')\mu' d\mu' \tag{5}$$

where E_S is the sky irradiance just below the surface. The final component considered, which is due to internal reflection of light beneath the surface, can be calculated after assuming the Fresnel reflectance at the water surface to be 1 for $\mu \leq \mu_c$ and 0 for $\mu > \mu_c$ using the following implicit integral equation.

$$\begin{aligned} L_I(\mu) = {} & 2\pi \int_0^{\mu_c} [L_S(\mu')+L_D(\mu',\mu_0)] R(\mu,\mu')\mu' d\mu' \\ & + 2\pi \int_0^{\mu_c} L_I(\mu')\, R(\mu,\mu')\mu' d\mu' \end{aligned} \tag{6}$$

The second integral in (6) can be reasonably approximated by

$$2\pi\, L_I(\mu_c) \int_0^{\mu_c} R(\mu,\mu')\mu' d\mu' \tag{7}$$

If one then evaluates (6) at $\mu=\mu_c$ and solves for $L_I(\mu_c)$ using (7) $L_I(\mu)$ becomes

$$\begin{aligned} L_I(\mu) = {} & 2\pi \int_0^{\mu_c} [L_D(\mu',\mu_0)+L_S(\mu')] R(\mu,\mu')\mu' d\mu' + 2\pi \int_0^{\mu_c} R(\mu,\mu')\mu' d\mu' \\ & \times 2\pi \int_0^{\mu_c} [L_S(\mu')+L_D(\mu',\mu_0)] R(\mu_c,\mu')\mu' d\mu' \\ & \times \left(1-2\pi \int_0^{\mu_c} R(\mu_c,\mu')\mu' d\mu'\right)^{-1} \end{aligned} \tag{8}$$

Applying equations (4) and (8) to each of the reflectance models listed above, individual expressions have been developed for components of $L_w(\theta,\theta_0)$ as shown in Table 2. Model calculated values of $L_w(\theta,\theta_0)$ at $\theta=0°$ were converted to above surface radiances $L_w^+(\theta, \theta_0)$ as

$$L_w^+(\theta,\theta_0) = 4n^{-1}(n + 1)^{-2}L_w(\theta,\theta_0) \qquad (9)$$

where n is the index of refraction of water. In the case of quasi single scattering it was assumed the phase function is uniform in the backward direction, i.e., $p(\mu) = 2\omega_0 B$ for $\mu<0$ where

$$B = \frac{1}{2\omega_0} \int_{-1}^{0} p(\mu')d\mu' \qquad (10)$$

is the backscattering frraction for the actual phase function $p(\mu)$.

Chandrasekhar [9] has formulated an exact solution for isotropic scattering. This solution can be adapted for highly forward scattering by considering the phase function $p(\mu,\phi,\mu',\phi')$ as the sum of delta and isotropic functions

$$p(\mu,\phi,\mu',\phi') = \omega_0 F'\delta(\mu-\mu')\delta(\phi-\phi') + 2\omega_0 B$$

where $F' = 4\pi(1-2B)$. Substitution of this phase function into the radiative transfer equation gives the same equation as in the case of isotropic scattering, except with ω_0 replaced by

$$\omega_0'=2\omega_0 B/(1 - \omega_0 F') \qquad (11)$$

The solution of this form of the radiative transfer equation is

$$R(\mu,\mu_0) = \frac{\omega_0' e}{4\pi(\mu+\mu_0)} H(\mu)H(\mu_0) \qquad (12)$$

TABLE 2. EXPRESSIONS FOR UPWELLING RADIANCE COMPONENTS[1]

Model	$R(\mu, \mu_o)$	$L_S(\mu)$	$L_I(\mu)$
Two Flow	$\dfrac{\omega_o B\pi^{-1}}{1-\omega_o F + [(1-\omega_o)^2 + 2\omega_o B(1-\omega_o)]^{1/2}}$	$E_S\ \pi^{-1}\ R(\mu,\mu_o)$	$\dfrac{(E_S + E_D)\pi^{-1}\ \mu_c{}^2\ R(\mu,\mu_o)}{1-\mu_c^2\ R(\mu,\mu_o)}$
Quasi-Single Scattering	$\dfrac{\omega_o B\pi^{-1}}{(\mu + \mu_o)(1 - \omega_o F)}$	$\dfrac{n^2 E_S\pi^{-1}\omega_o B[1-\mu_c-\mu L_N(\frac{\mu+1}{\mu+\mu_c})]}{1 - \omega_o F.}$	$\dfrac{x^2}{2\pi}\int_0^{\mu_c} (\frac{E_S}{\mu'+\mu_o} + \frac{E_D}{\mu'+\mu_1})\ \frac{\mu'\ d\mu}{\mu+\mu_1}$
Power Series Approximation	$R_1(\mu,\mu_o) = \sum_{n=0}^{N} a_n^1\ x^n\ \theta_o > 20°$ $R_2(\mu,\mu_o) = \sum_{n=0}^{N} a_n^2\ x^n\ \theta_o < 30°$ $[R_1(\mu,\mu_o) + R_2(\mu,\mu_o)]/2\ \ 20° \leq \theta \leq 30°$	$E_S\pi^{-1}\ R_2(\mu,\mu_o)$	$\dfrac{E_S\ \pi^{-1}R_2(\mu,\mu_o) + E_D\ R(\mu,\mu_o)}{[\mu_c{}^2\ R_2(\mu,\mu_o)]^{-1} - 1}$
Adapted Chandrasekhar	$\dfrac{\pi^{-1}\ \omega_o BH(\mu)\ H(\mu_o)}{2(\mu+\mu_o)[1-\omega_o(1-2B)]}$.	$2n^2 E_S \int_{\mu_c}^{1} R(\mu,\mu')\mu' d\mu'$ (by numerical integration)	$(L_D(\mu) + L_S(\mu)\ I^*(\frac{1+I^*-2\pi I^*}{1-2\pi I^*})$ $I^* = 2\pi \int_0^{\mu_c} R(\mu,\ \mu')\mu' d\mu'$ (by numerical integration)

[1] $\mu=\cos\theta$, ω_o = single-scattering albedo, B = backscatter probability, F = 1-B,
$x = \dfrac{\omega_o B}{1-\omega_o F}$, E_S = sky irradiance, E_D = direct irradiance, a_n^1 and a_n^2 from reference [4]

where H is given by an integral equation which can be numerically solved, and has been tabulated by Chandrasekhar [9]. We can now choose B such that for the measured phase function $p(\mu)$.

$$B = \frac{\int_{-1}^{0} p(\mu)d\mu}{\int_{-1}^{1} p(\mu)d\mu} \tag{13}$$

2.2 SIMULATION TECHNIQUES

Monte Carlo methods have been used by many investigators as a means to solve the radiative transfer problem for natural waters. Gordon has used Monte Carlo methods to derive the necessary coefficients for his power series model [4]. The power of the method lies in the fact that a solution can be obtained for a complex source, medium, and detector geometry which is beyond the limit of the existing simplified radiance models. In this sense the Monte Carlo approach represents our best opportunity to model the radiative transfer process of the measurement medium. Moreover Monte Carlo results can serve as a standard with which one can evaluate the significance of proposed or existing model simplifications and assumptions. It is for these reasons that application of Monte Carlo techniques were felt essential to the present study.

In Monte Carlo simulation one samples a sequence of events from known probability distributions from which the outcome or process distribution can be estimated. For the water medium the process becomes one of tracing the photon through a series of interactions where the photon is either scattered or absorbed at each interaction site. The scattering process is described uniquely by the single scattering albedo (ω_0) and the scattering phase function $\beta(\theta)$. If we trace a sufficient number of photons through the medium, good statistics can be obtained on those which emerge from the surface. However, the straight simulation, which is often referred to as "crude" Monte Carlo, is inefficient because most of the information is lost with those photons which are absorbed or contained by the medium. Thus substantial program efficiency can be achieved when information is retained by each photon interaction regardless as to the outcome of a photon trace. In our Monte Carlo procedure a number of techniques were employed to improve the efficiency with which acceptable statistics are realized. These techniques fall into two categories: (1) retention of information from photon histories, and (2) estimation of desired radiometric components from the accumulated photon statistics. In the first category it is useful to visualize a photon as a bundle of photon units. Using this concept we can determine the fraction of photons escaping from each interaction of the history. The technique which provides these estimations is called biasing. In this approach one distorts the true probability density function for a particular event in order to force the desired results. In order to prevent distortion of the sampling results a bias correction weight is applied to the photon bundle. The correction factor is calculated by comparing the probability distribution function of the distorted or biased events with the true probability distribution the correction factor or weight can be expressed as

$$W = \frac{dP_T(x)/dx}{dP_F(x)/dx} \tag{14}$$

where $P_T(x)$ and $P_F(x)$ are the true and false (biased) cumulative probability distribution functions [11].

There were two biasing techniques employed in our Monte Carlo code. The first called statistical estimation applies a series of weight adjustments to the photon to offset the fraction estimated to reach the surface. The distance between collisions is normally sampled from the distribution $e^{-\tau}$ where τ is the optical depth. With the statistical estimation procedure the photon remains in the medium to provide higher order results. Collisions can be forced by sampling from the density function

$$p(\tau)d\tau = \frac{e^{-\tau}}{1-e^{-\tau_m}} d\tau \quad 0 \leq \tau \leq \tau_m \tag{15}$$

In this case the sampling bias can be removed by multiplying the present weight (initially set to 1) by $1-e^{-\tau_m}$ which yields the fraction of photons remaining in the medium.

A second technique employed in the simulation was to bias the scattering function in the backward hemisphere. The method selected was to simply choose a backscatter coefficient B' which is larger than the actual coefficient B obtained by integrating the measured phase function. The appropriate weighing factors are then $W_F = F/F'$ (where $F' = 1-B'$) for the forward hemisphere and $W_B = B/B'$ for the backward hemisphere. Thus the biased phase function $p'(\mu)$ used for selecting scattering angles can be written as

$$p'(\mu) = \begin{cases} p(\mu)/W_F & 0 \leq \mu \leq 1 \\ p(\mu)/W_B & -1 \leq \mu < 0 \end{cases} \tag{16}$$

and the cumulative distribution function as

$$P'(\mu) = \begin{cases} P(\mu)/W_F & 0 \leq \mu \leq 1 \\ F' + (P(\mu) - F)/W_B & -1 \leq \mu < 0 \end{cases} \tag{17}$$

where $P(\mu)$ is the actual cumulative distribution function. For this case the photon weighting factors are simply

$$W(\mu) = \begin{cases} W_F & 0 \leq \mu \leq 1 \\ W_B & -1 \leq \mu < 0 \end{cases} \tag{18}$$

Thus a separate bias technique was employed for each of the two sampling distributions utilized at a photon interaction.

In the Monte Carlo code scattering angles were selected by solving the equation $P'(\mu) = r$ for μ, where r is a random number from the [0,1] interval. Values of $x = 1 - \mu$ were interpolated from tabulated values of P' using the equation

$$x = \left[\sqrt{x_i} - \frac{P_i - r'}{P_i - P_{i-1}} \left(\sqrt{x_i} - \sqrt{x_{i-1}} \right) \right]^2 \qquad (19)$$

which is defined for the interval $P_{i-1} \leq r \leq P_i$ and is appropriate for a concave distribution function. In equation 19, $r' = W_F \cdot r$ when $0 \leq r \leq F'$ and $r' = W_B(r-F') + F$ when $F' < r \leq 1$.

A third technique which was started but not fully implemented under the present contract is described as a semi-analytical method where a complete set of Monte Carlo photon histories are obtained for a typical phase function. Results can then be calculated for any similar phase functions by computing the proper weights for each history. With this method all of the matrix transformation calculations required in the standard procedure for each interaction are eliminated saving great quantities of computer time.

A second category of Monte Carlo techniques includes those which improve the accuracy of and flexibility to select radiometric parameters. Photons emerging within the critical angle are recorded by scattering order and zenith angle. It is convenient to enter all photons for the medium from zenith. Since the bidirectional reflectance $R(\theta,\phi,\theta',\phi')$ is symmetrical in θ and θ' by means of reciprocity the incident and reflected angle can be reversed [9]. Thus the reflectance of direct incident light from any solar zenith angle can be determined for zenith view angle. The radiance reflectance $R(\theta, 0)$ is now easily calculated with the following expression.

$$R(\theta,0) = 2\pi \sum_{k=1}^{k=IMAX} \frac{N^*(\theta,k)}{N} \omega_o^k + R_N \qquad (20)$$

where N is the number of incident photons, ω_o^k is the probability of k^{th} order scattering, $N^*(\theta, k)$ is a cubic spline interpolation of the Monte

Carlo bias function $n(\theta_i, k)$, and R_N is the contribution from all orders higher than IMAX. In order to estimate R_N we first assume $N^*(\theta, k)/N$ as a function of k has form $a.b^k$ where a and b are constants to be determined. It follows that R_N can be written as

$$R_N = a \sum_{k=0}^{\infty} b^k - a \sum_{k=0}^{IMAX} b^k \tag{21}$$

$$= \frac{a}{1-b} - a(1 + b + b^2 + \ldots. + b^{IMAX})$$

$$= \frac{ab^{IMAX + 1}}{1 - b}$$

$c = ab^{IMAX} = N^*(\theta, IMAX)/N$ is known so $R_N = \frac{cb}{1-b}$, $b = R_N/(c+R_N)$

and $a = N^*(k)/Nb^k$

Thus R_N can be calculated for any ω_o as

$$R_N = \frac{a(b\omega_o)^{IMAX}}{1-b\omega_o} \tag{22}$$

For radiance calculations it is convenient to assume that higher orders are isotropic beneath the surface. The diffuse hemispherical reflectance for zenith incident light can be readily calculated from (20) as

$$R_H(0) = 2 \int_0^{\pi/2} R(0,\theta) \cos\theta \sin\theta \, d\theta \tag{23}$$

The Monte Carlo program was validated by making comparisons between the simulation results and those obtained from exact solutions. For both linear and isotropic scattering the radiative transfer equation has been solved by Chandrasekar [9]. Monte Carlo simulations were run for both of these scattering functions using 20,000 photons incident from the zenith. Simulated hemispherical reflectances compare well to exact values, as shown in Figure 1, over a wide range of single scattering albedos. Calculated reflectances $R(\theta, 0) = \pi L(\theta, 0)/E$ are compared in Figures 2 through 4 for selected values of ω_0 and view angle. While the radiance reflectances also compare quite well there is a small amount of noise apparent in these Monte Carlo results as a function of view angle. These small discrepancies may be due in part to convergence problems. Convergence of the simulation code was examined for selected scattering functions, and bidirectional and hemispherical reflectance were estimated for 100 to 20,000 photons as presented in Figure 5. A similar analysis was made for the Back River scattering function at 450 nm as shown in Figure 6. As might be expected, bidirectional reflectances require a substantially greater number of photons to achieve convergence than hemispherical reflectances. There appear to be long period components remaining in the bidirectional reflectance functions after 100,000 photons. Thus, it is considered possible to minimize the minor discrepancies shown in Figures 5 and 6 by conducting the simulations up to 100,000 photons beyond which the value of further reduction is questionable.

Besides the number of photons, several other input parameters were investigated prior to beginning the simulation analysis on LaRC optical measurements. These studies included determining how large the biasing could become without distorting the results and determining the maximum number of interactions. One criterion set up to observe the effects of these selections was the number of photons required to approach the final value to within five percent. The use of biasing techniques do not directly save computer time. For example, the costs of running a 100,000 photon simulation are approximately the same. Savings are realized in that fewer photons are required to meet, say, a five percent convergence criteria. Several biasing ratios were tried with linear, Gordon Type B, and back River (B450) phase functions with inconclusive results other than a biasing ratio of two appears to produce satisfactory simulation results for a variety of functions tested and thus reduce the photon requirements by one-half to 50,000.

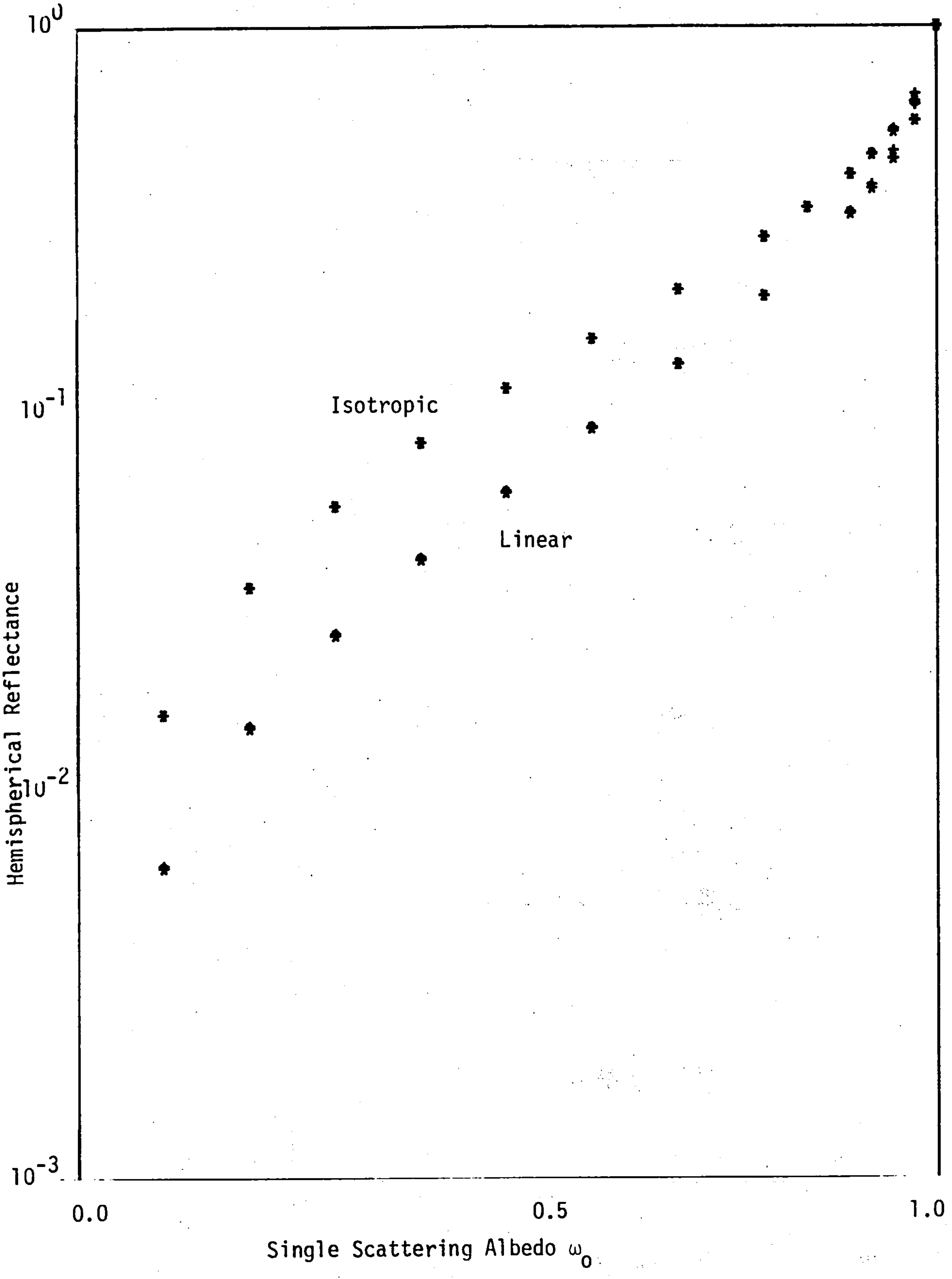

Figure 1. Comparison of Hemispherical Reflectance as Predicted by Monte Carlo (+) with Exact Solutions (*) as a Function of ω_o for Linear and Isotropic Scattering.

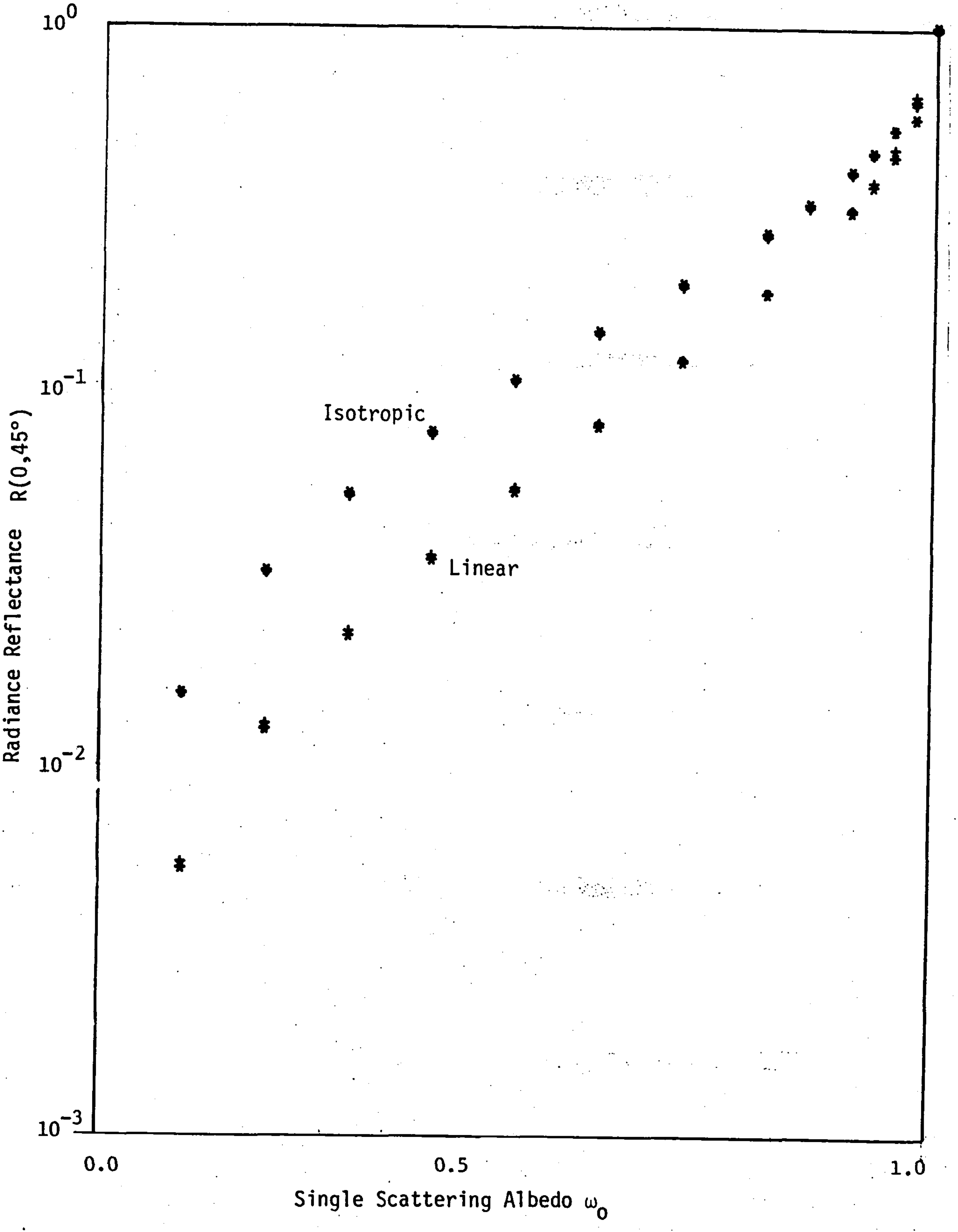

Figure 2. Comparison Radiance Reflectance as Predicted by Monte Carlo (+) with Exact Solutions (*) as a Function of ω_0 for Linear and Isotropic Scattering.

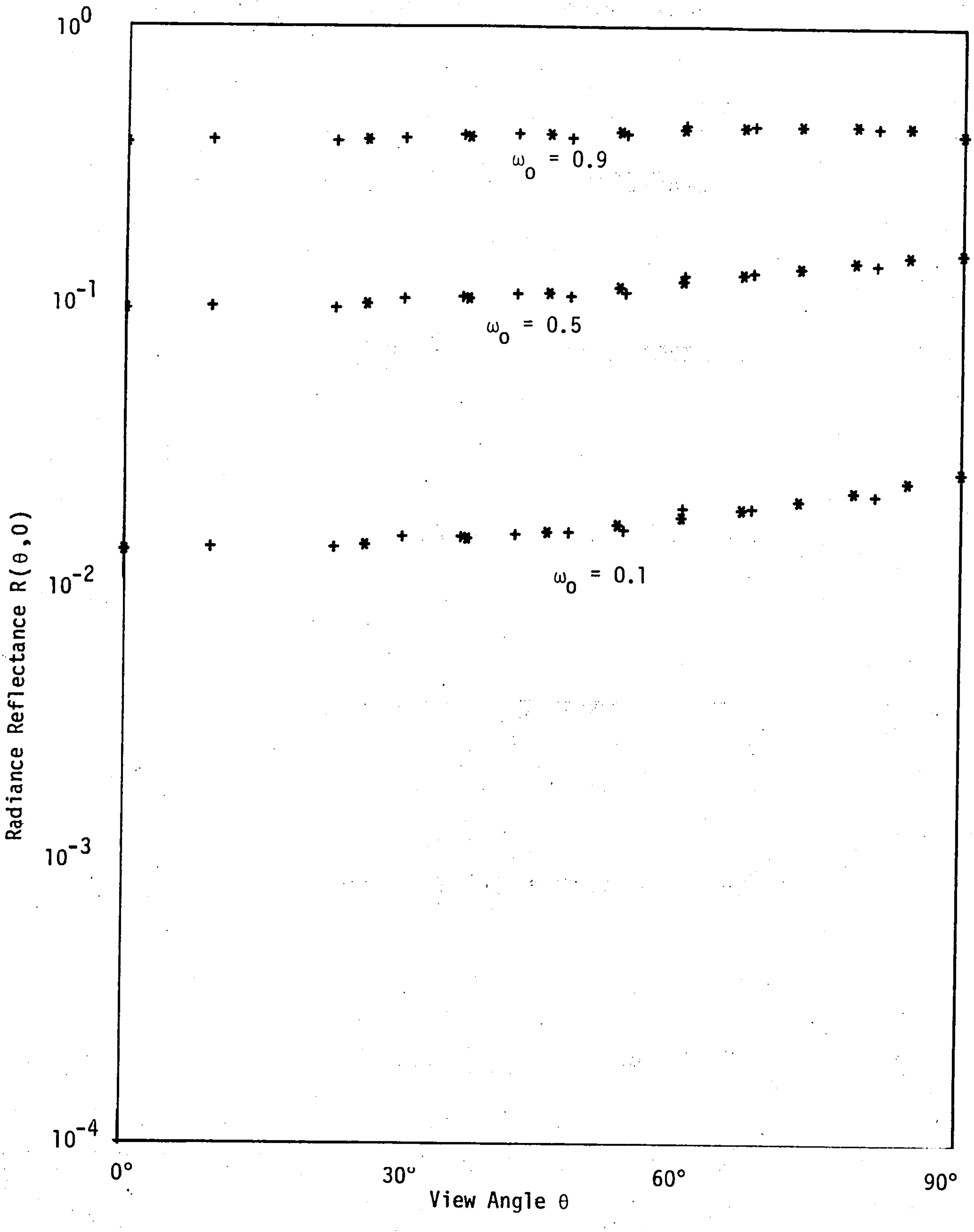

Figure 3. Comparison Radiance Reflectance as Predicted from Monte Carlo Results (+) with Exact Solutions (*) as a Function of View Angle for Isotropic Scattering ($p(\theta) = \omega_o$)

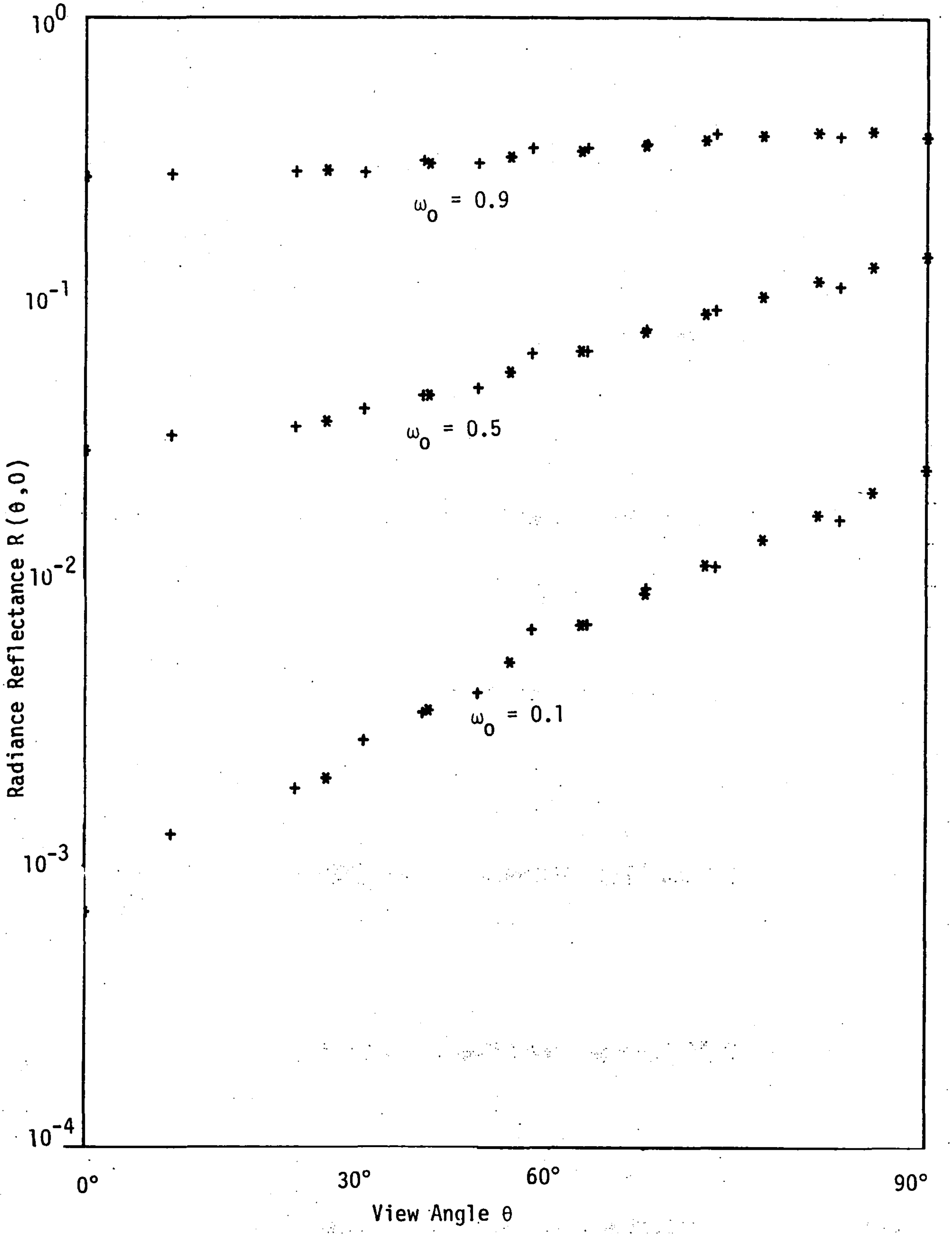

Figure 4. Comparison of Radiance Reflectance as Predicted from Monte Carlo Simulation (+) with Exact Solutions (*) as a Function of View Angle for Linear Scattering ($p(\theta) = (1+\cos\theta)\cdot\omega_o$)

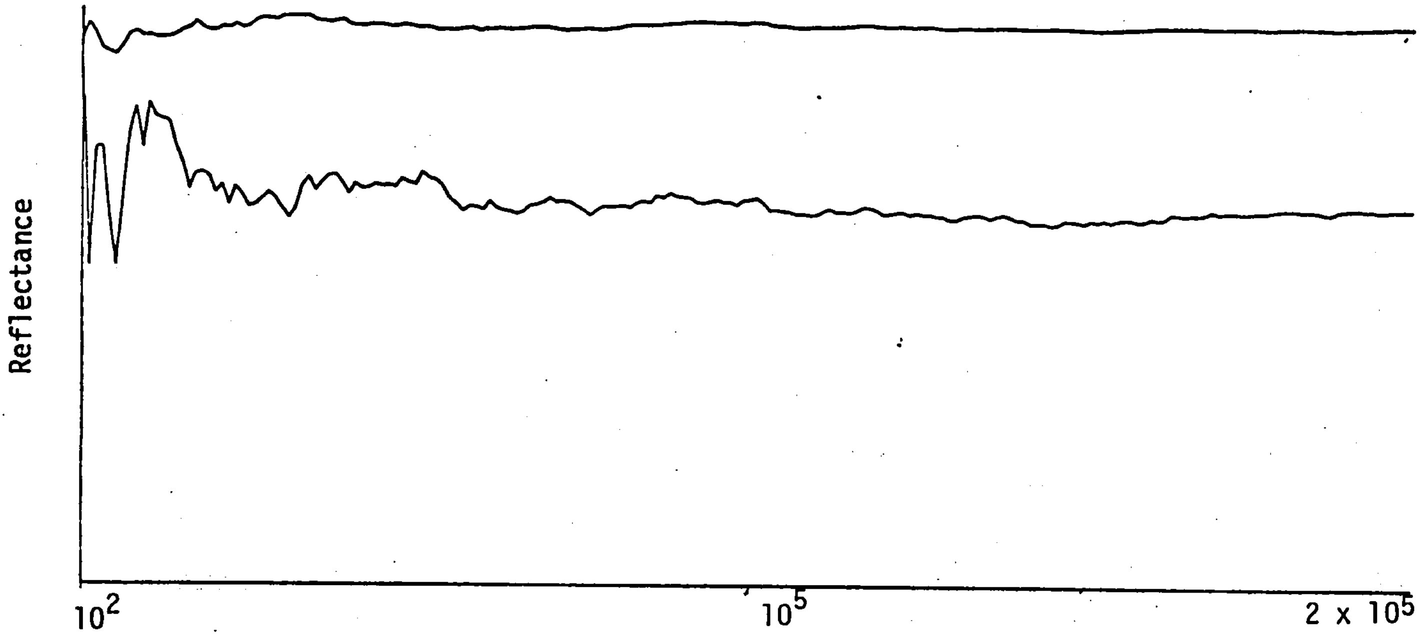

Figure 5. Crude Monte Carlo Predicted Isotropic Hemispherical (upper curve) and Bidirectional (lower curve) Reflectances as a Function of Number of Photons. Bidirectional Reflectance is from 39.2 to 45.0 degrees.

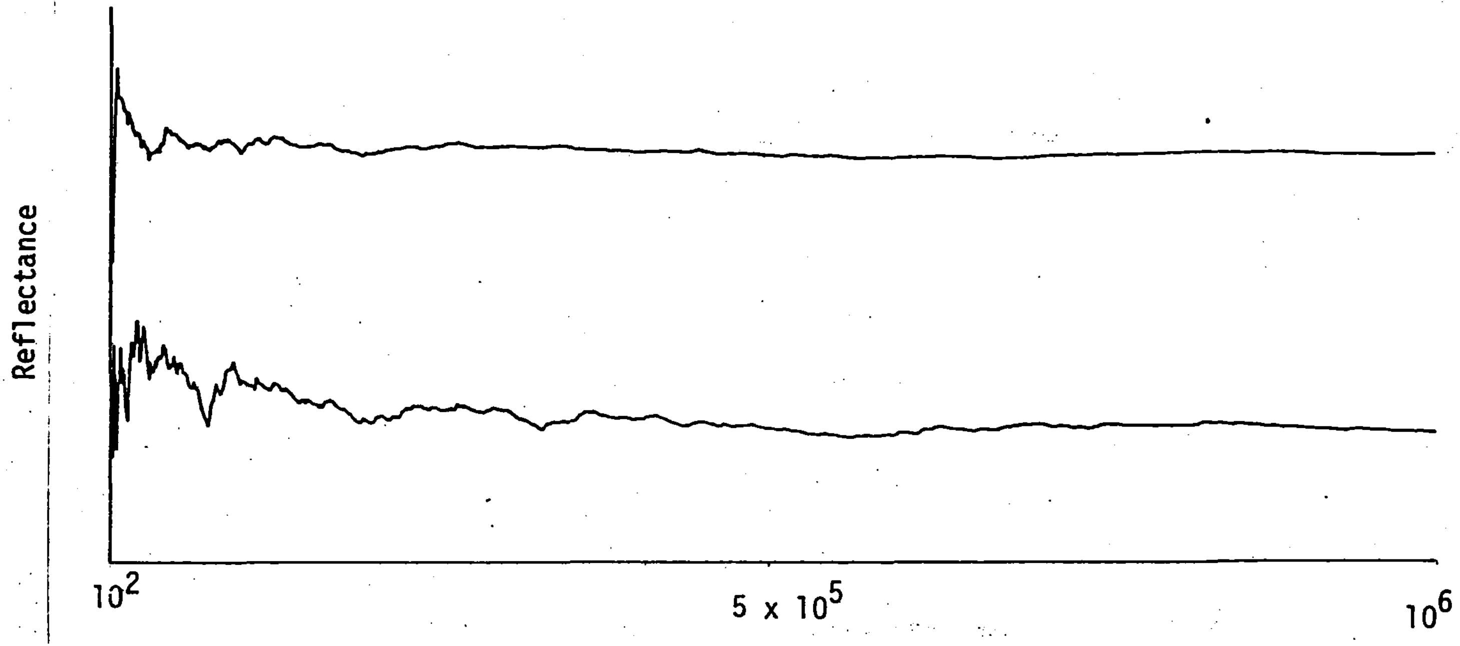

Figure 6. Crude Monte Carlo Predicted Hemispherical (upper curve) and Bidirectional (lower curve) Reflectances as a Function of Number of Photons. Simulations Utilized Back River Measured Phase Function at 450 nm. Bidirectional Reflectance is from 0.0 to 18.4 degrees.

The effect of variable number of photon interactions is shown in Table 3, both with and without the estimated contribution from higher orders. There is a steady increase in reflectance with the number of interactions permitted. Convergence to the final value is obtained with fewer interactions when the higher order estimate is included. Our studies indicated that twenty interactions were sufficient to obtain reliable results.

TABLE 3

COMPARISON OF HEMISPHERICAL (R_H) AND BIDIRECTIONAL R(0,35°) REFLECTANCES WITH AND WITHOUT HIGHER ORDER ESTIMATION FOR VARIOUS MAXIMUM NUMBER OF INTERACTIONS

Maximum Number of Interactions	Reflectance Without Higher Order Estimates		Reflectance With Higher Order Estimates	
	R_H	R(0,35°)	R_H	R(0,35°)
10	2.637	0.891	5.763	1.940
20	4.271	1.392	6.066	1.994
30	5.139	1.695	6.133	2.029
40	5.577	1.843	6.006	1.987

THIS PAGE INTENSIONALLY LEFT BLANK

3.0

RESULTS AND INTERPRETATION

Each of the water radiance models was applied to the measured optical data set and the predicted upwelling radiance spectra were compared with measured values. Given the value of absorption and backscatter these models predict the reflectance below the surface. The predicted above-surface radiance was calculated using the methods described in section 2 and the measured irradiance.

The Monte Carlo simulation model required the use of the entire scattering phase function. In order to produce comparable results it was important that the measured optical parameters should be self consistent in the sense of equation (1). While it is recognized that there are errors associated with each of measured optical properties the greatest absolute uncertainty was connected to the measurement of b as an integration of $\beta(\theta)$ since a significant portion of $\beta(\theta)$ lies between small angle and large angle portions as measured by two different instruments (1.5° to 25°).

For this study the integral of $\beta(\theta)$ was calculated by Gaussian quadrature after cubic spline functions were fitted to the measured values of $\beta(\theta)$. It was found that the resulting integral was highly sensitive to the values selected at both ends of the unmeasured segment of $\beta(\theta)$. With small adjustments to $\beta(\theta)$ of less than five percent the integral could be brought into exact agreement with c and a producing the desired consistent data set. The backscatter coefficient remains constant under this type of adjustment to $\beta(\theta)$ which Gordon [4] has reported will have little effect on volume reflectance.

Values of the backscatter probability and the single scattering albedo ω_0 together with the measured irradiances shown in Table A2 were used to calculate each of the radiance spectra presented in Figures 7-9. The Monte Carlo simulations were made at each 50 nm interval using

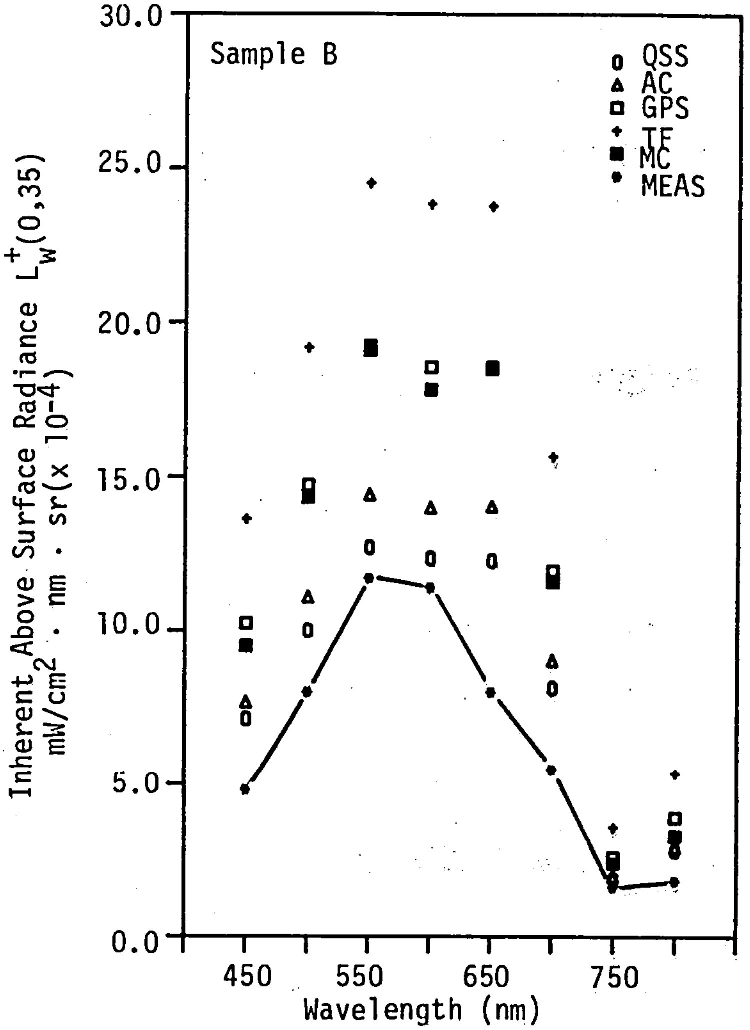

Figure 7. Comparison of Observed and model predicted upwelling radiance for Sample B

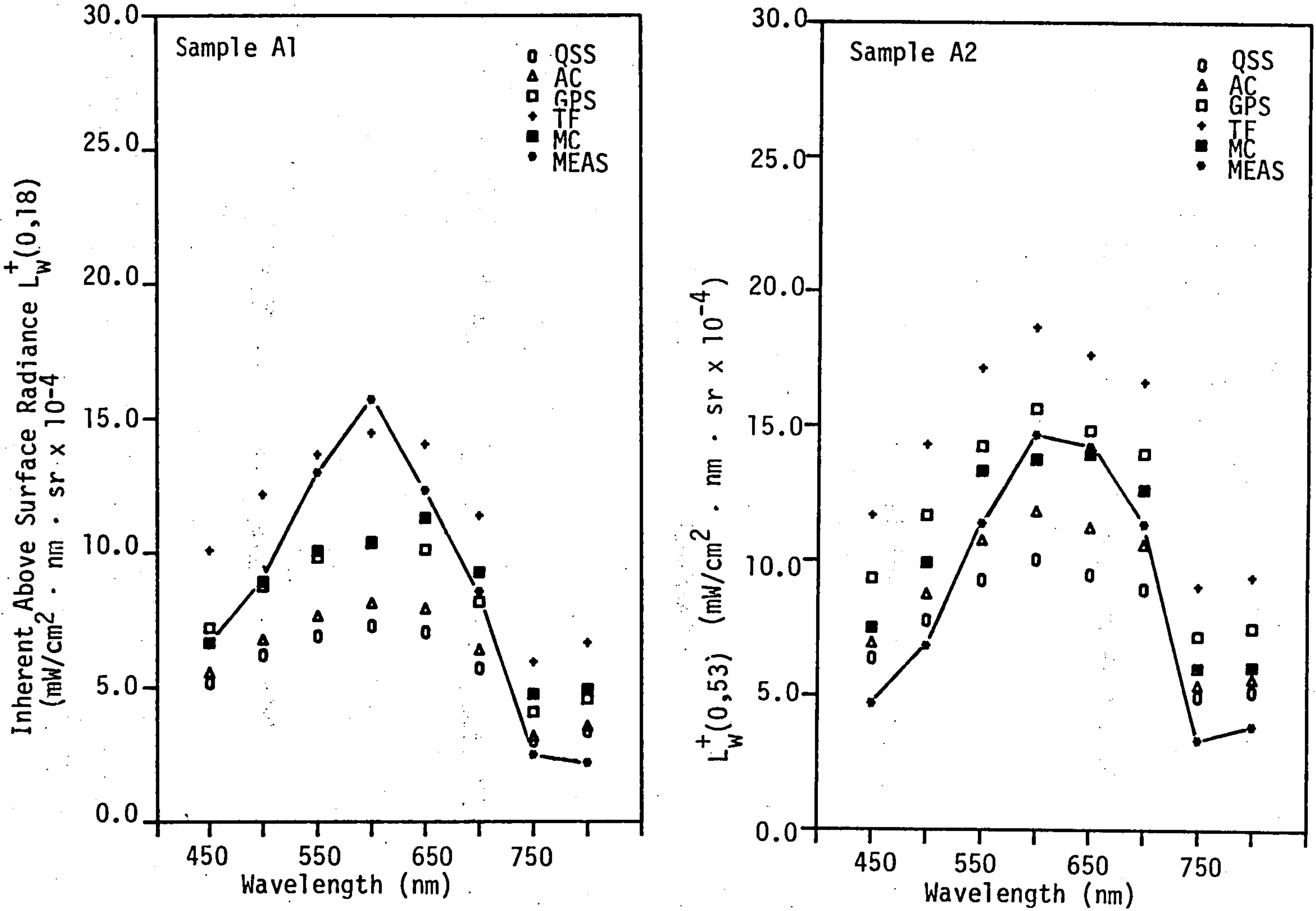

Figure 8. Comparison of observed and model predicted upwelling radiance for samples A1 and A2

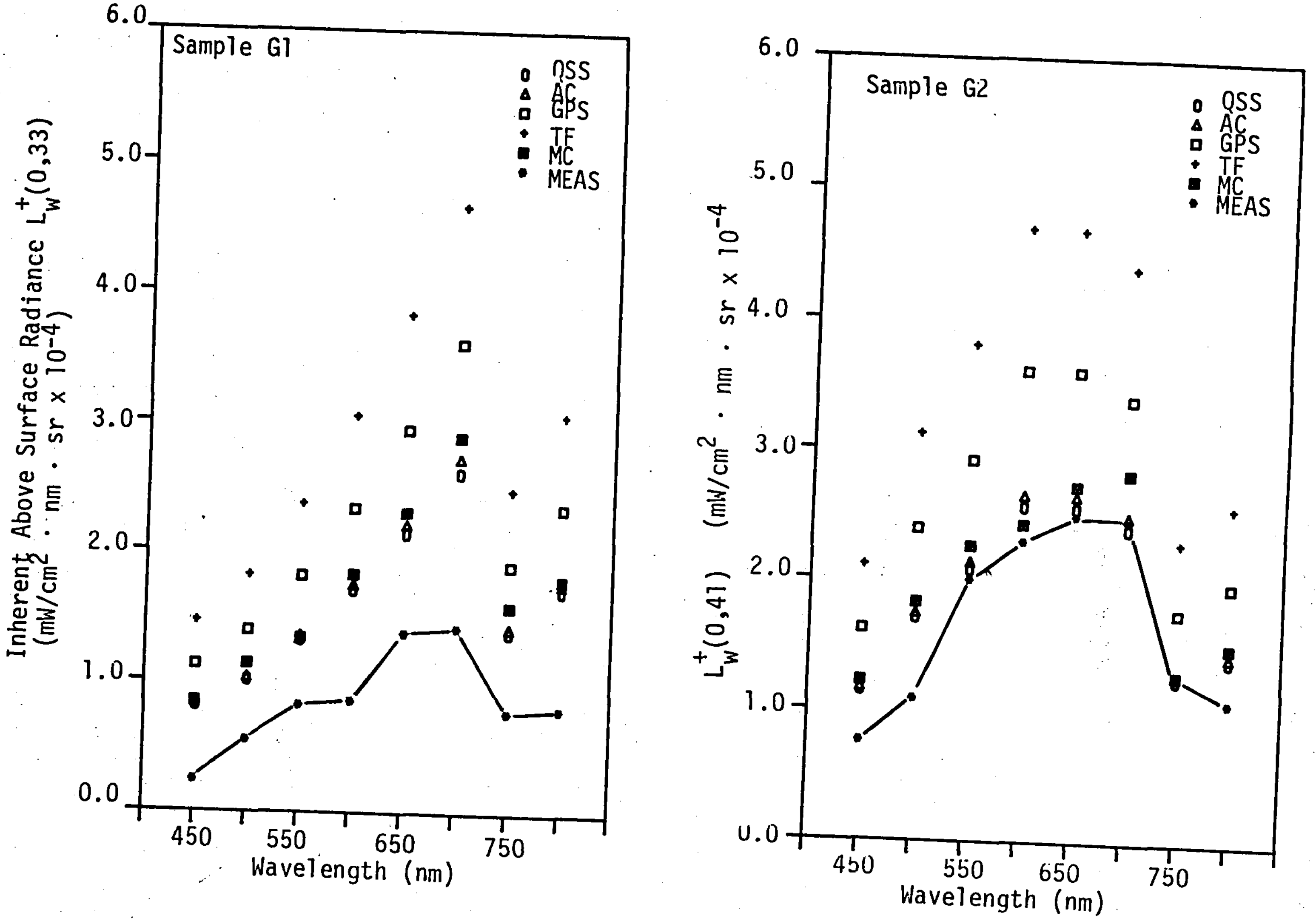

Figure 9. Comparison of Observed and Model Predicted Upwelling Radiance for Samples G1 and G2

50,000 photons. A maximum of twenty interactions was permitted in each simulation. The contribution from higher orders was estimated with an exponential fit of the first twenty orders.

3.1 COMPARISON OF MODEL CALCULATIONS

Model predicted inherent radiances above the surface $L_W^+(\theta,\theta_0)$ are compared to measured values of upwelling radiance in Figures 7 through 9 for each of the five test cases.

In cases B, G1, and G2 the model predicted values had similar spectral shape to the measured values but were frequently less than fifty percent of the Monte Carlo predictions. Waters for test sites G1 and G2 had very low inherent reflectances, thus the upwelling signal contained a relatively larger specular component. As a result determination of the measured inherent radiance was in these cases more doubtful. For cases A1 and A2 the measured radiances had substantially different spectral shape as compared to model predicted values. These differences are also evident in Figures 10 and 11 which compare the Monte Carlo and Gordon Power Series predictions to measured values.

The model predictions displayed the following order from the smallest to largest predicted values: QSS, AC, MC, GPS, and TF. The spread in these predictions as the figures indicate was large and some predictions were several times the measured radiances. The various models reflected individual sensitivities to the optical parameters although in general there is a consistent relationship between the optical parameter as shown in Appendix A and the predicted radiances. The Monte Carlo predictions did not in all cases approximate the same simplified model results. For cases G1 and G2 the adapted Chandrasekhar and quasi single scattering models closely approximated the Monte Carlo calculations while in cases B, A1, and A2 the Gordon Power Series more closely fits the Monte Carlo results. For all cases the spectral shape produced by the power series approximation and the Monte Carlo results is nearly the same as indicated by the comparison made in Figure 12.

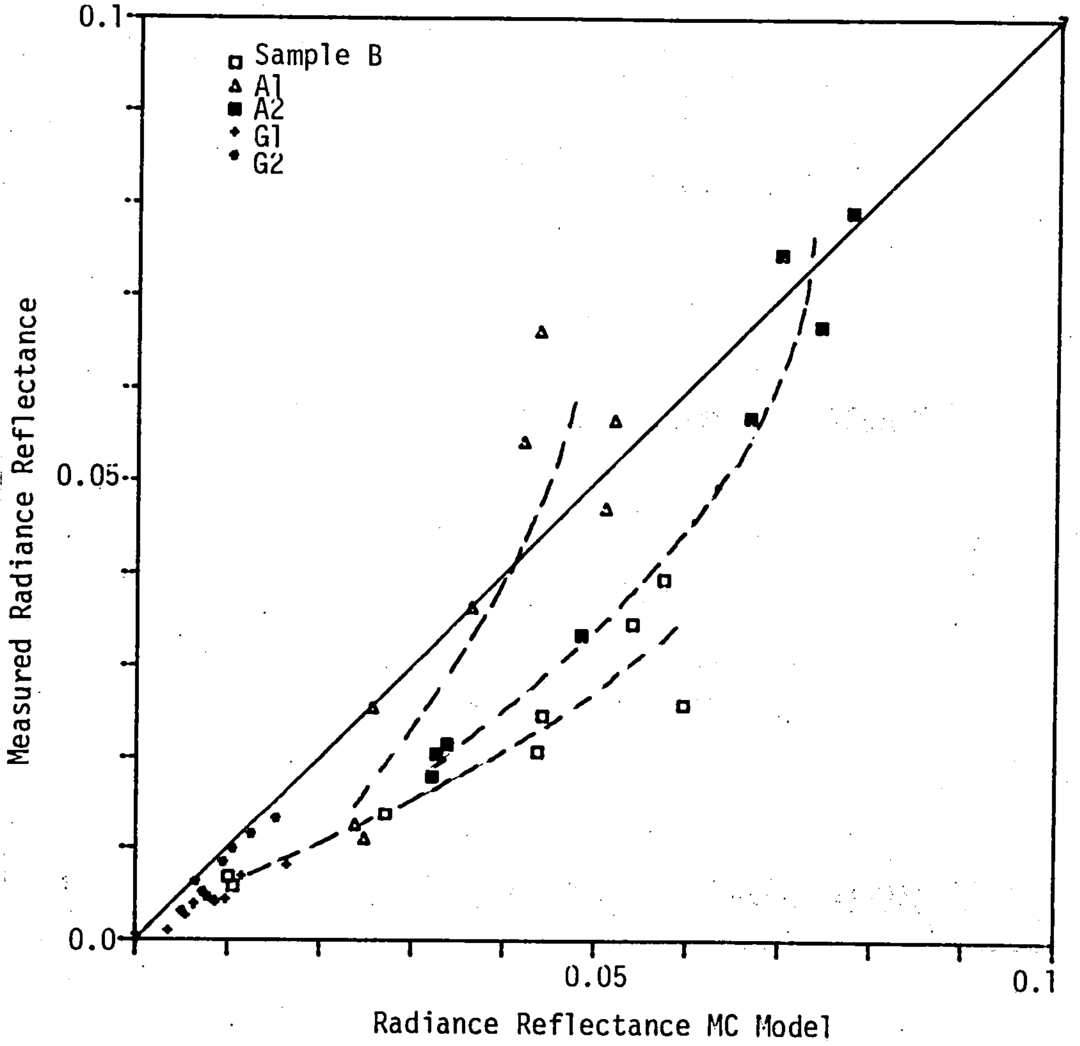

Figure 10. Measured versus Monte Carlo Predicted Reflectance

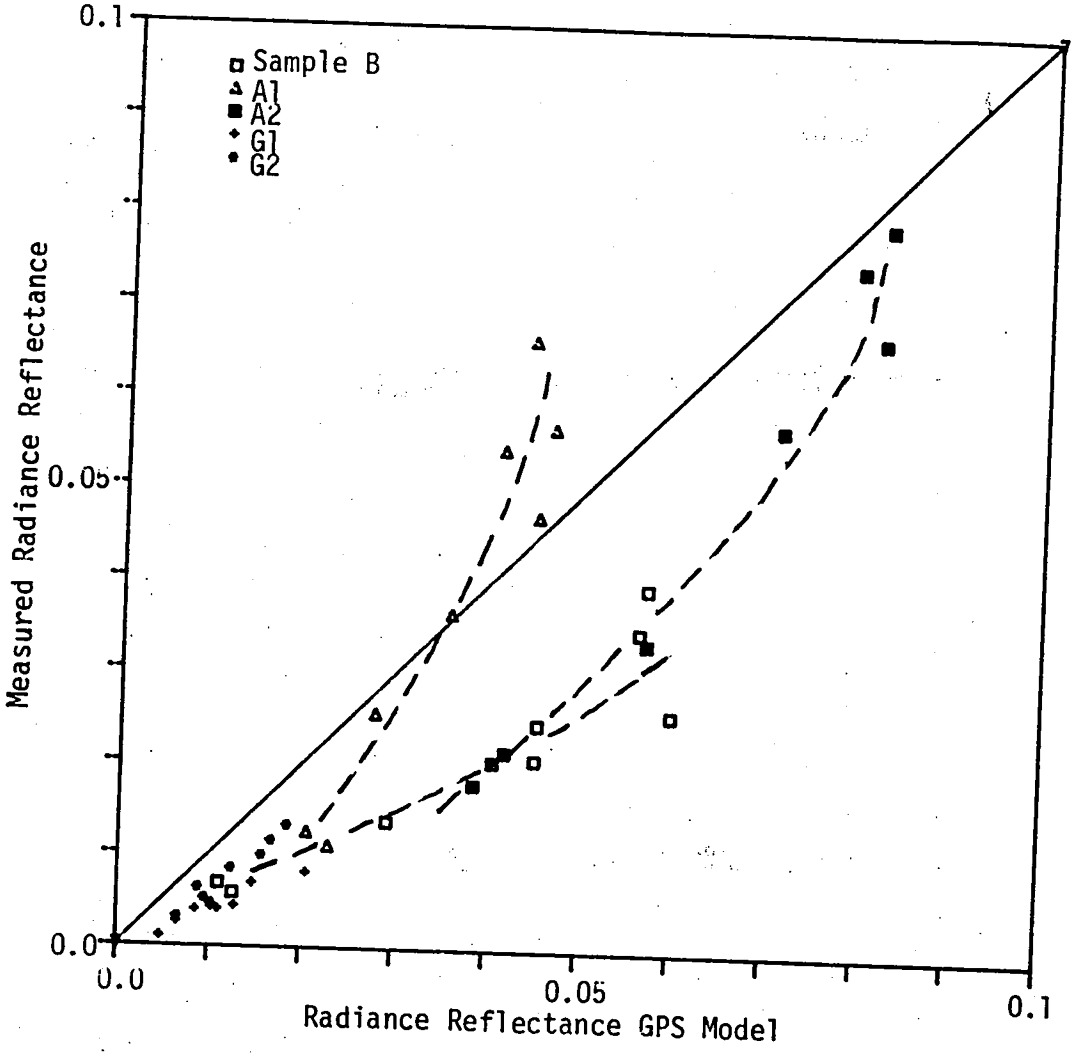

Figure 11. Measured versus GPS Model Predicted Reflectance

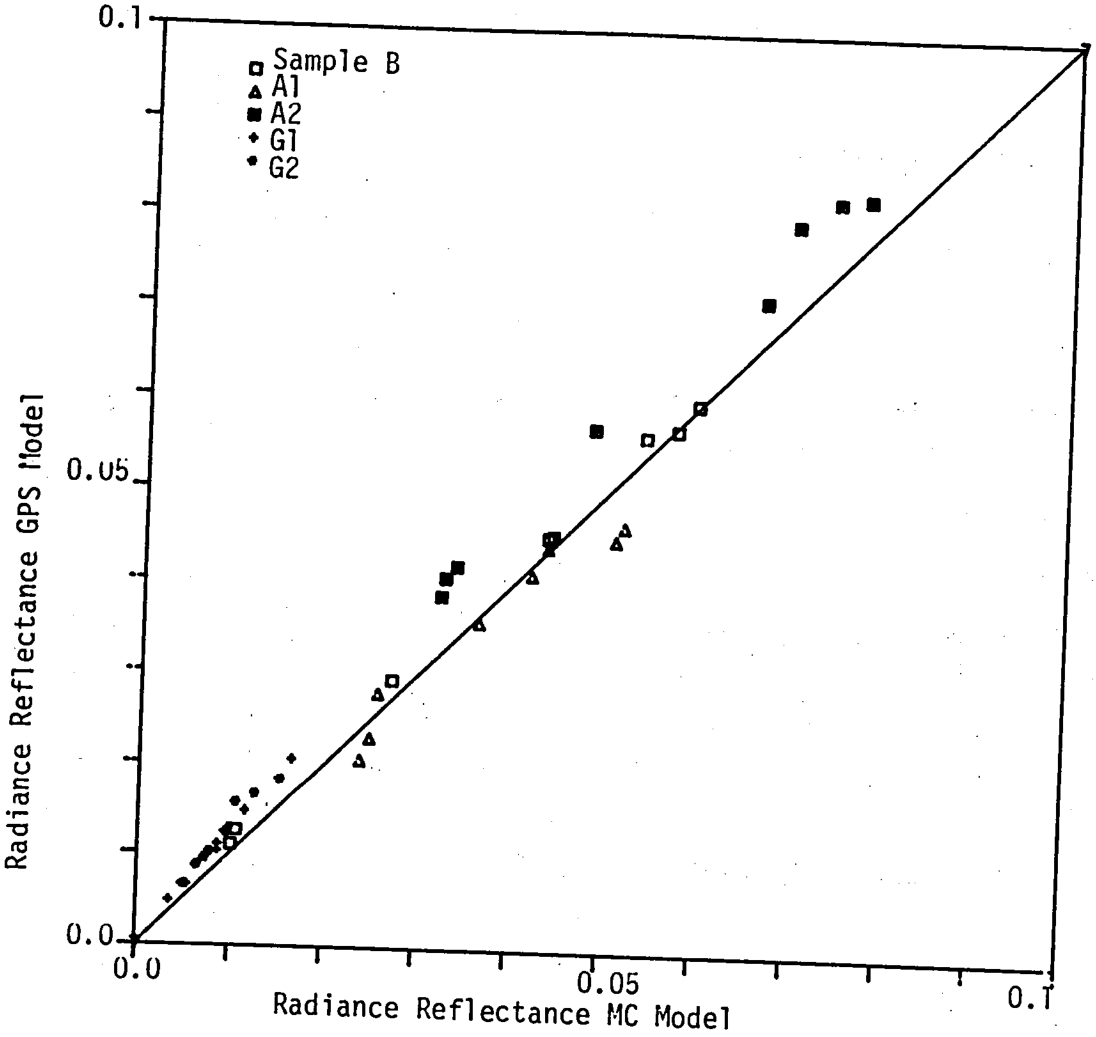

Figure 12. GPS versus Monte Carlo Model Predicted Reflectance

The peaks of the model predicted and measured radiance spectra occurred at 600 nm for cases B, A1, and A2 and 675 to 700 nm for cases G1 and G2. This spectral shift in the peak is suspected to be largely due to the presence of a high dissolved organics component in these latter samples.

It is difficult to account for the discrepancies between the measured and model predicted radiances. There are at least four possible sources of error which could account for the observed lower values of radiance. These are (1) instrumentation measurement errors, (2) changes in particle size distribution, (3) sampling errors due to unknown stratifications, and (4) failure of the model to properly account for photon interactions with the water suspended solids.

Instrumentation errors associated with the measurement of optical properties and the above surface upwelling radiance cannot in our estimation completely account for the observed differences. The nearly consistent set of optical properties obtained at most of the wavelengths suggests very small errors are present in these results. The high sampling rate of the Tektronix J20 spectrometer provides excellent statistics for each measurement taken. Since this instrument was also used to measure the downwelling irradiance possible errors in absolute calibration are not critical to the data relationships shown in Figures 7-9. Errors due to surface effects would tend to average out with the rapid sampling rate.

Since the optical properties were determined from the presence of chlorophyll and suspended materials it is conceivable that the sample underwent changes between the time of collection and time of the laboratory optical measurements. During this intervening time period the sample could have undergone changes in biological state, particle disassociation, or aggregation. A decrease in chlorophyll-a concentration would cause a slight increase in reflectance over time as would any break up of phytoplankton cellular or organic materials. A loss of mineral or organic particles by aggregation or attachment to container walls may be associated with a decrease in reflectance. This latter contention is based upon Mie scattering theory. Mie scattering cross section depends on the number of size of particles with a corresponding greater weight (scattering efficiency) given to smaller particles. Thus with say a decrease in the number of smaller particles there is a corresponding decrease in B. Since $x = Bb/(a + Bb)$ is nearly linear with reflectance, a reduction in sample reflectance should be expected. In a highly unlikely case where all particles disassociated into equal subparticles the shape of the particle size distribution would remain the same and the reflectance would increase by approximately twenty-five percent.

Since the Gordon Power Series approximation was based upon Monte Carlo results it was of interest to further examine predictions made by these two models. As shown in Table 2, Gordon Power Series approximation gives two different reflectance functions, R_1 for hemispherical reflectance of direct incident sunlight from zenith and R_2 for hemispherical reflectance for diffuse incident skylight. Gordon indicates that R_2 approximates the reflectance of direct sunlight for solar zenith angles greater than 30°. The Monte Carlo results describe the upward irradiance distribution for direct incident light from zenith. The radiance reflectance for isotropic diffuse incident light is numerically equivalent to the hemispherical reflectance for direct incident light from zenith. Thus if the illumination distribution were isotropic then the Monte Carlo and GPS results should be equivalent.

Predicted upward radiance as calculated by Gordon's Power Series approximation is compared with Monte Carlo radiances in Figure 13 as a function of the solar zenith angle. These calculations were made using the test site B absorption and scattering properties. The hump in the power series results is due to a combination of the Fresnel transmittance through the air/water interface and change from R1 to R2 over the

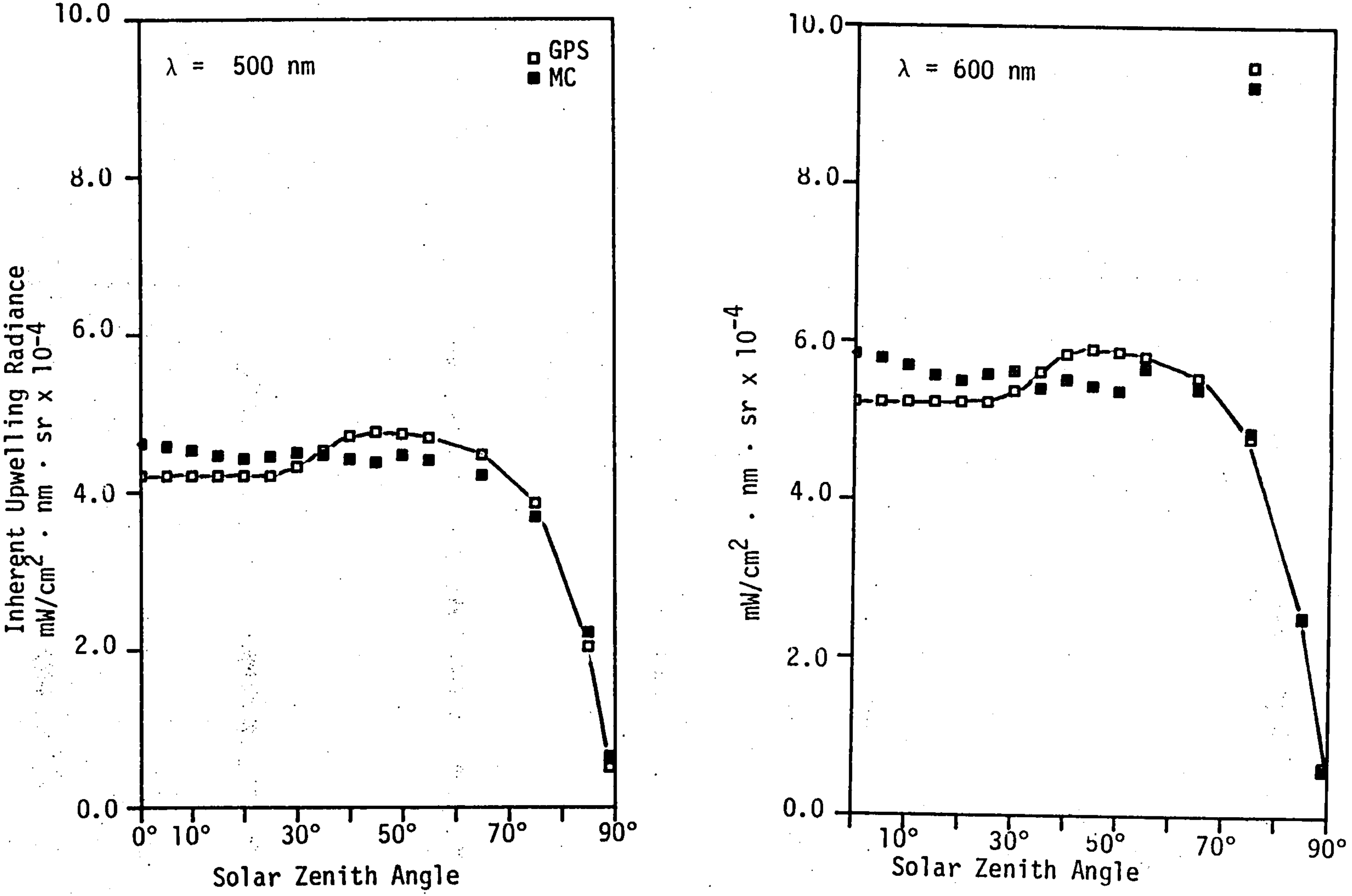

Figure 13. Comparison of Gordon's Power Series Approximation (GPS) with Monte Carlo (MC) Calculated Radiance versus Solar Zenith Angle for Sample B

20° to 30° angle interval. The Monte Carlo simulations tended to predict slightly larger radiances for small values of the solar zenith angle which generally decrease with some fluctuations slowly to 65° and then fall off rapidly as the Fresnel coefficient. The closest approximations occurred in the angular region of cross over and for angles greater than 75°. Additional comparisons are contained in Appendix B for test sites A1 and G1. The nonuniformities of the Monte Carlo curves are pronounced in these latter comparisons. It is not known whether these variations are solely due to sampling errors or to actual variants in the upward irradiance distribution.

Gordon analysis [4] did not include large single scattering albedos which were calculated for most of the present data as shown in Table A1. Figure 14 compares the below surface hemispherical reflectance for the GPS to the Monte Carlo simulations as a function of Bb/(a + Bb) with values of the scattering albedo ranging from 0.1 to 0.98. Reflectances shown compare well to a Bb/(a+Bb) value of 0.2 ($\omega_0 \approx 0.9$) where the GPS predicted reflectances begin to underestimate those predicted by Monte Carlo. Additional comparisons are shown in Appendix B.

3.2 USE OF WATER OPTICAL PROPERTIES TO EXTRACT CONSTITUENT CONCENTRATIONS

As was briefly discussed in the beginning of this report the ultimate goal of this research is the development of a methodology which can be applied to satellite or airborne remote sensing data to gain quantitative information on specific water pollutants. Some past studies conducted by this laboratory and other have focused on empirical relationships which are calibrated to an area of interest with a requirement for extensive surface truth information. In the present approach inherent optical properties of a water type or constituent are used to define an algorithm which will reduce observed upwelling spectral radiance into value of constituent concentration. If a sufficiently large body of optical properties are available for dominant constituent it is possible

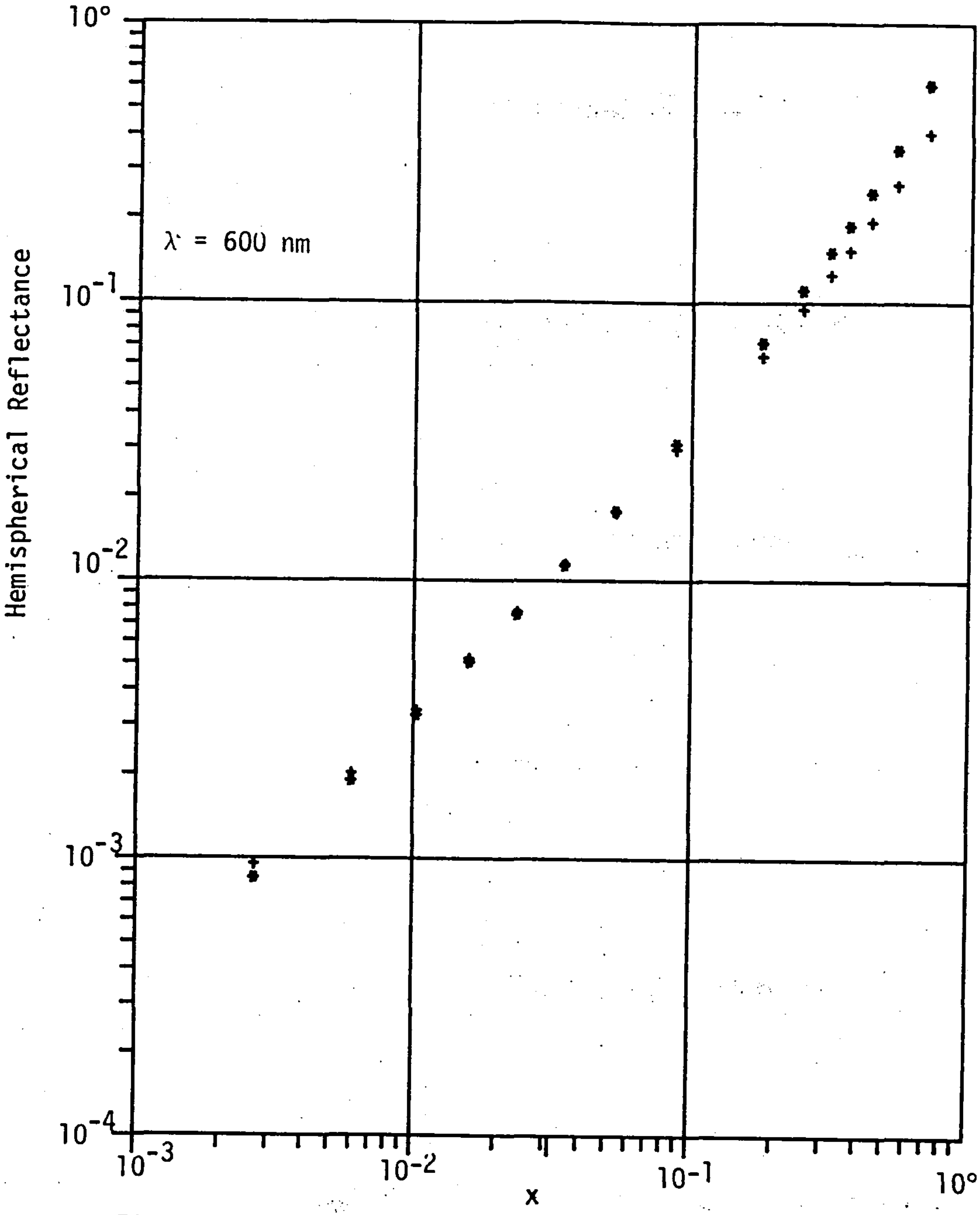

Figure 14. GPS Model (+) and Monte Carlo (*) Predicted Below Surface Hemispherical Reflectances versus the parameter. $x=Bb(a+Bb)^{-1}$. Sunlight is direct and Incident from Zenith. Sample B Optical Properties were Used for These Calculations.

that an algorithm can be applied to specific remote sensing data with only very minimal requirements for surface truth data.

Ideally one needs to have knowledge of the optical properties of each component in a given water matrix in order to resolve concentration information from reflectance data. The radiance reflectance can be easily related to constituent concentration using say the Gordon Power Series since both a and Bb are additive over constituent concentrations, i.e.,

$$\begin{aligned} a &= a_W + \sum_i \hat{a}_i \, c_i \\ Bb &= (Bb)_W + \sum_i (\hat{Bb})_i \, c_i \end{aligned} \tag{24}$$

where a_W and $(B)_W$ are the absorption and backscattering coefficients of pure water and $\hat{a}_i$ and $(\hat{Bb})_i$ are the specific coefficients for the ith constituent. Thus, if we know the optical properties and concentrations it would become straightforward to predict the reflectance. However, to obtain concentrations from optical coefficients is a complex procedure and one that is expected to be highly sensitive to noise in the radiometry. A more practical solution is to examine the multivariate relationship between concentration and reflectance over appropriate wavelengths. Over limited ranges of concentration it is possible to approximate the reflectance with simple mathematical relationships. In order to derive a specific algorithm for airborne or satellite radiometric data four separate models must be considered. These are (1) instrumentation calibration model, (2) an atmospheric model which removes all transmittance and path radiance effects, (3) an air/water interface model which removes specular reflectance and transmittance effects, and (4) a water radiance model which can accurately predict inherent radiance reflectance based upon the optical properties of major constituents.

The determination of specific optical properties from a set of measurements made on samples with various mixtures of constituents may be a difficult task. If quantities of unknown materials are present they could have a significant impact on the measured optical characteristics. Under such circumstances application of linear regression techniques will require many individual sample measurements in order to obtain satisfactory results. Alternatively it may be possible to determine the optical properties of a particular constituent in the presence of unknown materials with addition of known quantities of the constituent.

THIS PAGE INTENSIONALLY LEFT BLANK

4.0

CONCLUSIONS AND RECOMMENDATIONS

4.1 CONCLUSIONS

Field measurements of inherent optical parameters from five very turbid water test sites have been used to make a preliminary evaluation of five water reflectance models for use in predicting upwelling radiance. These models included Monte Carlo simulations which are considered to provide the best opportunity to imitate the radiative transfer process. Measured radiance spectra and model predictions were found to compare well only in selected cases and wavelengths. In general the measured radiances were well below predicted values. Reflectance models tested with the optical data gave widely varying predictions but with apparent interrelationships between individual predictions at a given wavelength. Possible factors which may have caused the observed discrepancies include (1) anisotropic characteristics of the diffuse sky radiance distribution, (2) instrumentation errors, (3) temporal changes in the water sample use for *in vitro* optical measurements, (4) relative size and variability of the specular and inherent components of the measured upwelling radiance, and (5) inadequacies of existing reflectance models as applied to turbid waters. However, a complete explanation for these discrepancies is not apparent from the available site data. Samples A2 (Appomattox River) and G2 (Ogeechee River) provided the best comparisons between model generated and measured radiances with differences typically less than twenty-five percent. None of the models produced consistently good comparisons for all five test sites.

4.2 RECOMMENDATIONS

Based upon the experience gained in the present study and the research goals there are four types of studies which should be included in future programs. These studies would enhance our understanding of the radiative transfer process in very turbid waters and improve our ability to relate the inherent optical properties to the concentrations of principal constituents.

1. Measure the angular distribution of incident irradiance. Employ Monte Carlo simulation techniques to investigate the influence of anisotropic irradiance on the upwelling vertical radiance.

2. Measure the temporal and spatial changes in water optical conditions at a given test site with an in situ beam transmittance meter. Examine the reproducibility of optical measurements from similar samples.

3. Determine the variability of natural particle size distributions ($N_p = Ad_p^{-7}$) in a given water body and analyze the influence of change in various particle size frequency on measured scattering properties.

4. Conduct a system study designed to predict constituent concentration in the presence of background conditions. Determine how precise and extensive optical measurements must be made in order to ascertain concentrations from reflectance data over the entire water body.

REFERENCES

1. Whitlock, Charles, et al., Comparison of reflectance with backscatter and absorption parameters for turbid waters. Applied Optics, Vol. 20, No. 3, page 517, February 1, 1981.

2. Jerlov, N.G., Optical Oceanography, Elsevier, page 70, New York, 1968.

3. Petzold, T.J., Volume scattering functions for selected waters, Scripps Institution of Oceanography, University of California at San Diego, 1972.

4. Gordon, H.R., Brown, O.B., and Jacobs, M.M., Computed relationships between inherent and apparent optical properties of a flat homogeneous ocean, Applied Optics, Vol. 14, p. 417, February 1975.

5. Gordon, H.R., Simple calculation of the diffuse reflectance of the ocean, Applied Optics, Vol. 12, p. 2803, December 1973.

6. Jain, S.C. and Miller, J.R. Algebraic expression for the diffuse irradiance reflectivity of water from the two-flow model, Applied Optics, Vol. 16, p. 202, January 1977.

7. Plass, G.N., Humphreys, T.J., and Kattawar, G.W., Color of the ocean, Applied Optics, Vol. 17, p. 1432, May 1978.

8. Cherdak, A., Friedman, E. An absorption coefficient instrument for water: Concept, fabrication, calibration. NASA CR-158955, November 1978.

9. Chandrasekhar, S., Radiative transfer, Dover Publications, New York, 1960.

10. Ghovanlou, A. Radiative transfer model for remote sensing of suspended sediments in water. NASA Report CR 145145, February 1977.

11. Gordon, H.R., et al. Introduction to ocean optics, SPIE Ocean Optics VI, Vol. 208, 1979.

APPENDIX A

WATER OPTICAL MEASUREMENTS

This appendix contains measured optical properties (Table A1), field radiance measurements (Table A2), and measured scattering function (Table A3) for each of the five sampling test sites, Appomattox River (A1 and A2), Back River (B), Satilla River (G1), and Ogeechee River (G2). The individual angular scattering measurements for A1, A2, and B have been reported in [1] and will not be repeated here.

In the water radiance model calculations it was considered essential that optical data set be self-consistent, that is, as these parameters are interrelated according to the following equation

$$\hat{c} - \hat{a} = 2\pi \int_0^{\pi} \hat{\beta}(\theta) \sin\theta \, d\theta \qquad \text{(A-1)}$$

In a single test sample it is unlikely that these three independent measurements would be equatable.

The primary measurement uncertainty is due to the large angular sampling gap between the large angle measurements ($\geq$ 25°) the small angle measurements (< 1.5°). The volume scattering coefficient, calculated by numerical integration of $\beta(\theta)$, is sensitive to the curve fit between gap points. Our approach to the integration of $\beta(\theta)$ was to fit the measurement points with a series of cubic spline functions. These functions can then be interpolated to obtain a sufficient number of points for numerical integration. The cubic spline routine allows adjustment of the 0° and 180° end points.

An interactive code PHASEFIT was developed to make a cubic spline fit to the measured values of $\beta(\theta)$, provide a means of making small adjustments to the values of $\beta(\theta)$ where necessary, perform the above integration, and plot the adjusted scattering phase function. Scattering

TABLE A1
MEASURED OPTICAL PROPERTIES

	λ_{nm}	$c(m^{-1})$	$a(m^{-1})$	$b(m^{-1})$	B	ω_0
Sample A1	450	20.30	3.69	16.61	.0363	.8182
	500	17.78	2.72	15.06	.0389	.8472
	550	15.85	2.09	13.76	.0381	.8684
	600	14.33	1.83	12.50	.0398	.8726
	650	13.34	1.53	11.81	.0377	.8850
	700	12.70	1.64	11.06	.0416	.8707
	750	13.83	3.38	10.45	.0391	.7558
	800	12.56	2.93	9.63	.0394	.76678
Sample A2	450	27.54	6.42	21.12	.0686	.7668
	500	22.52	4.02	18.50	.0713	.8214
	550	18.86	2.71	16.88	.0707	.8566
	600	16.39	2.09	14.30	.0700	.8727
	650	14.70	1.80	12.90	.0701	.8772
	700	13.42	1.74	11.68	.0743	.8703
	750	14.42	3.52	10.90	.0684	.7558
	800	12.67	2.96	9.71	.0703	.7667
Sample B	450	11.28	1.52	9.84	.0256	.8648
	500	10.09	0.89	9.27	.0255	.9118
	550	9.30	0.64	8.64	.0250	.9314
	600	8.90	0.60	8.35	.0242	.9325
	650	8.56	0.52	8.05	.0231	.9395
	700	8.40	0.74	7.66	.0253	.9119
	750	10.17	2.96	7.19	.0243	.7089
	800	8.97	2.51	6.42	.0265	.7197
Sample G1	450	23.80	14.51	9.29	.0376	.3902
	500	16.81	8.51	8.30	.0349	.4935
	550	12.51	5.28	7.23	.0326	.5780
	600	10.08	3.61	6.47	.0320	.6421
	650	8.45	2.43	4.71	.0312	.7129
	700	7.46	1.68	5.78	.0319	.7745
	750	8.67	2.96	4.24	.0278	.6590
	800	7.34	2.16	4.09	.0279	.7055
Sample G2	450	16.75	9.18	7.57	.0405	.4517
	500	12.70	5.16	7.54	.0358	.5934
	550	10.08	3.63	6.45	.0356	.6401
	600	8.70	2.84	5.86	.0393	.6736
	650	7.70	2.14	5.56	.0331	.7227
	700	7.16	1.86	5.30	.0336	.7397
	750	8.62	3.45	5.17	.0299	.6000
	800	7.47	2.88	4.59	.0305	.6143

TABLE A2
FIELD RADIANCE MEASUREMENTS

	λ_{nm}	E_{DIRECT}(mW/nm . cm^2)	$E_{DIFFUSE}$(mW/nm . cm^2)	L_w^+(mW/nm.cm^2.sr)
Sample A1**	450	588	229	6.6
	500	601	169	8.9
	550	634	120	13.0
	600	647	97	15.7
	650	617	68	12.3
	700	521	51	8.6
	750	578	50	2.5
	800	614	46	2.2
Sample A2**	450	478	245	4.7
	500	477	167	6.8
	550	515	113	11.4
	600	531	87	14.7
	650	503	62	14.2
	700	481	53	11.3
	750	534	53	3.3
	800	525	40	3.9
Sample B	450	858	242	4.8
	500	845	176	8.0
	550	924	129	11.7
	600	920	116	11.4
	650	895	79	8.0
	700	778	55	5.5
	750	693	46	1.6
	800	877	97	1.8
Sample G1	450	587	157	0.24
	500	537	123	0.55
	550	577	83	0.86
	600	604	62	0.86
	650	581	47	1.38
	700	520	33	1.42
	750	537	41	0.78
	800	522	57	0.80
Sample G2	450	563	207	0.76
	500	576	162	1.09
	550	617	130	2.0
	600	620	108	2.3
	650	600	85	2.5
	700	525	60	1.27
	750	563	65	1.09
	800	562	91	

*Adjusted for specular reflectance of diffuse skylight (see page 5)

**Diffuse Irradiance estimated as discussed on page A-5.

Table A3. Volume Scattering Function Values

	θ, deg	450	500	550	600	650	700	750	800
	0.37400E+00	.22910E+04	.18513E+04	.15200E+04	.13121E+04	.11602E+04	.10748E+04	.92013E+03	.81765E+03
	0.75100E+00	.10597E+04	.87983E+03	.73561E+03	.63717E+03	.46983E+03	.52007E+03	.45532E+03	.40436E+03
	0.14900E+01	.32157E+03	.29253E+03	.25272E+03	.20373E+03	.19423E+03	.18819E+03	.14868E+03	.14594E+03
	0.25000E+02	.13148E+01	.11652E+01	.10090E+01	.81006E+00	.84078E+00	.81972E+00	.74429E+00	.68503E+00
	0.30000E+02	.87680E+00	.74672E+00	.64461E+00	.51853E+00	.60061E+00	.51951E+00	.46879E+00	.42658E+00
	0.45000E+02	.34533E+00	.29349E+00	.24646E+00	.22350E+00	.19857E+00	.19513E+00	.17421E+00	.15848E+00
ple G1	0.60000E+02	.17677E+00	.14709E+00	.12054E+00	.93635E-01	.95928E-01	.93077E-01	.83006E-01	.74641E-01
	0.75000E+02	.10361E+00	.86348E-01	.70173E-01	.62521E-01	.55166E-01	.53567E-01	.46572E-01	.42818E-01
	0.90000E+02	.70098E-01	.58487E-01	.46996E-01	.41881E-01	.36888E-01	.35857E-01	.30776E-01	.28466E-01
	0.10500E+03	.56984E-01	.46344E-01	.37289E-01	.33301E-01	.29171E-01	.28433E-01	.24349E-01	.22590E-01
	0.12000E+03	.51971E-01	.42490E-01	.34019E-01	.31140E-01	.26875E-01	.26305E-01	.22682E-01	.02313E-01
	0.13500E+03	.50916E-01	.42730E-01	.34300E-01	.31003E-01	.27355E-01	.26464E-01	.23013E-01	.20602E-01
	0.15000E+03	.53154E-01	.45645E-01	.37218E-01	.30348E-01	.28154E-01	.29692E-01	.25590E-01	.23585E-01
	0.15500E+03	.55073E-01	.47155E-01	.39962E-01	.32442E-01	.33171E-01	.33271E-01	.28539E-01	.26132E-01
	0.37400E+00	.29165E+04	.23864E+04	.20334E+04	.17858E+04	.15705E+04	.14848E+04	.13118E+04	.11956E+04
	0.75100E+00	.13436E+04	.11446E+04	.98969E+03	.89612E+03	.68245E+03	.76258E+03	.68474E+03	.63466E+03
	0.14900E+01	.41647E+03	.37717E+03	.33900E+03	.27976E+03	.24747E+03	.26750E+03	.21328E+03	.21131E+03
	0.25000E+02	.11525E+01	.10659E+01	.92917E+00	.85287E+00	.79504E+00	.74604E+00	.68896E+00	.61995E+00
	0.30000E+02	.78956E+00	.71529E+00	.60928E+00	.54599E+00	.50244E+00	.48047E+00	.44084E+00	.39039E+00
	0.45000E+02	.31497E+00	.27459E+00	.23659E+00	.23929E+00	.18892E+00	.18386E+00	.16374E+00	.14547E+00
ple G2	0.60000E+02	.15758E+00	.13648E+00	.11450E+00	.10374E+00	.92547E-01	.88175E-01	.75944E-01	.67938E-01
	0.75000E+02	.89777E-01	.79839E-01	.67359E-01	.68072E-01	.52688E-01	.50625E-01	.44520E-01	.39260E-01
	0.90000E+02	.61553E-01	.53477E-01	.44994E-01	.45430E-01	.35464E-01	.33732E-01	.29671E-01	.26465E-01
	0.10500E+03	.48871E-01	.42679E-01	.35434E-01	.36533E-01	.28536E-01	.27178E-01	.23862E-01	.21514E-01
	0.12000E+03	.44722E-01	.39268E-01	.33233E-01	.34561E-01	.26314E-01	.25351E-01	.22075E-01	.20103E-01
	0.13500E+03	.44668E-01	.39687E-01	.33797E-01	.34548E-01	.27118E-01	.26183E-01	.22521E-01	.19989E-01
	0.15000E+03	.47680E-01	.42418E-01	.36595E-01	.33616E-01	.29906E-01	.29356E-01	.25076E-01	.22747E-01
	0.15500E+03	.50327E-01	.45390E-01	.40431E-01	.36986E-01	.32836E-01	.32602E-01	.27936E-01	.25823E-01

functions given in figures A1 through A5 show the final fitted curve and degree of point adjustment.

The total irradiance was measured by viewing a horizontal Lambertian 99% reflector coated with Eastman 6080 white reflectance paint. Since the calculated reflectance is somewhat different for direct and diffuse irradiance, it was deemed necessary to estimate these two components of the total irradiance. The procedure adopted for this eatimation was to assume the sky radiance to be uniform (i.e., isotropic). Thus, the diffuse irradiance was obtained by multiplying this sky radiance by π, and the direct irradiance was obtained by subtracting the diffuse from the total irradiance.

For Case A1 the measured vertical sky radiance exceeded the total white card radiance and, therefore, the card radiance is an unrepresentative measure of the diffuse sky radiance. This effect may have been caused by the presence of broken clouds and/or a small solar zenith angle which provided a partial view of the solar aureole. The Case A2 sky radiance was also found to be high. In both cases the diffuse irradiance was estimated to be some fraction of the total as prescribed by Jerlov [2] for a particular wavelength and solar elevation angle. In all other cases the diffuse irradiance was estimated at π times the measured vertical sky radiance.

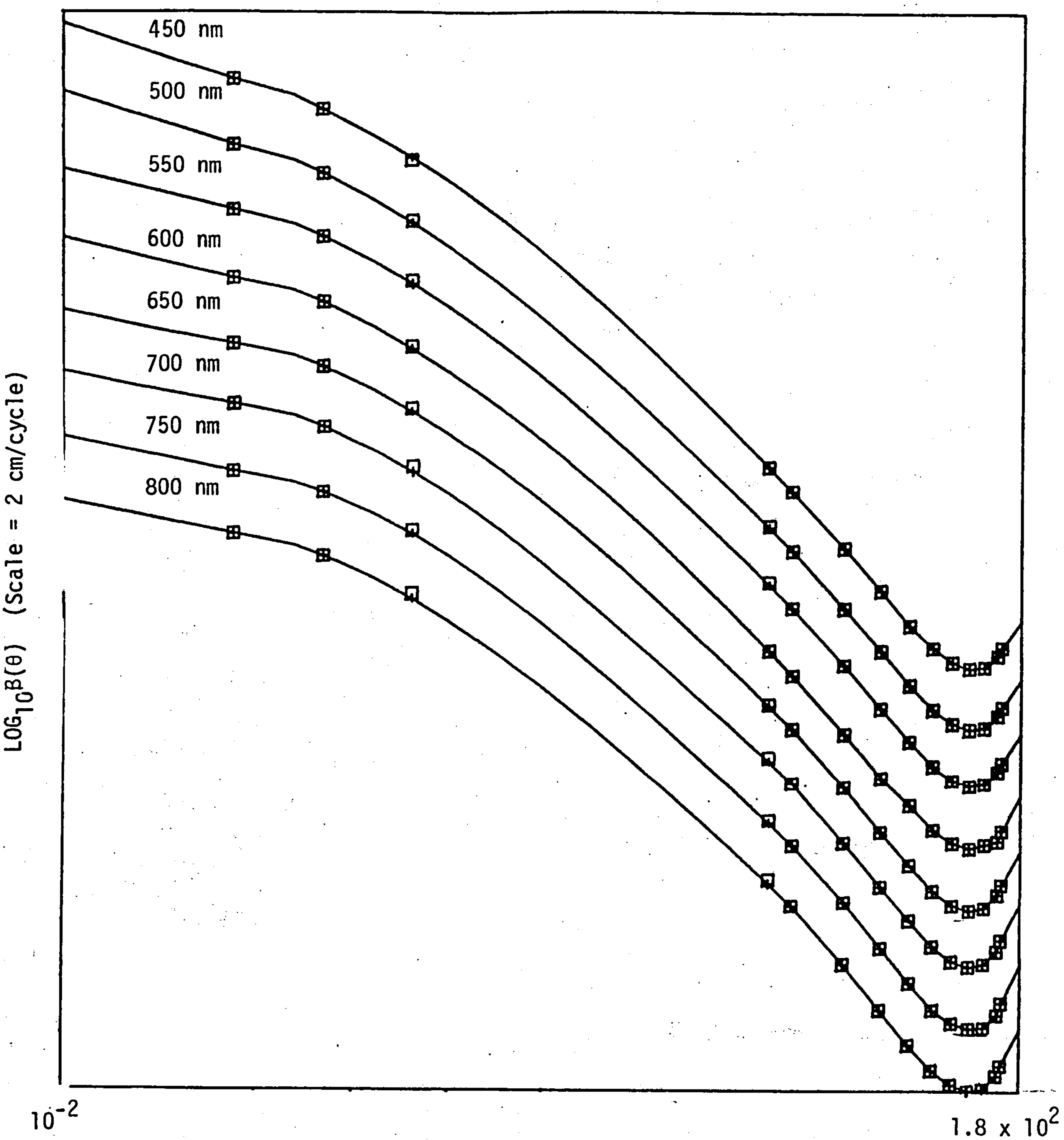

Figure A1. Volume scattering function β(θ) versus scattering angle θ for sample A1. Squares are centered on measured data and crosses on adjusted values.

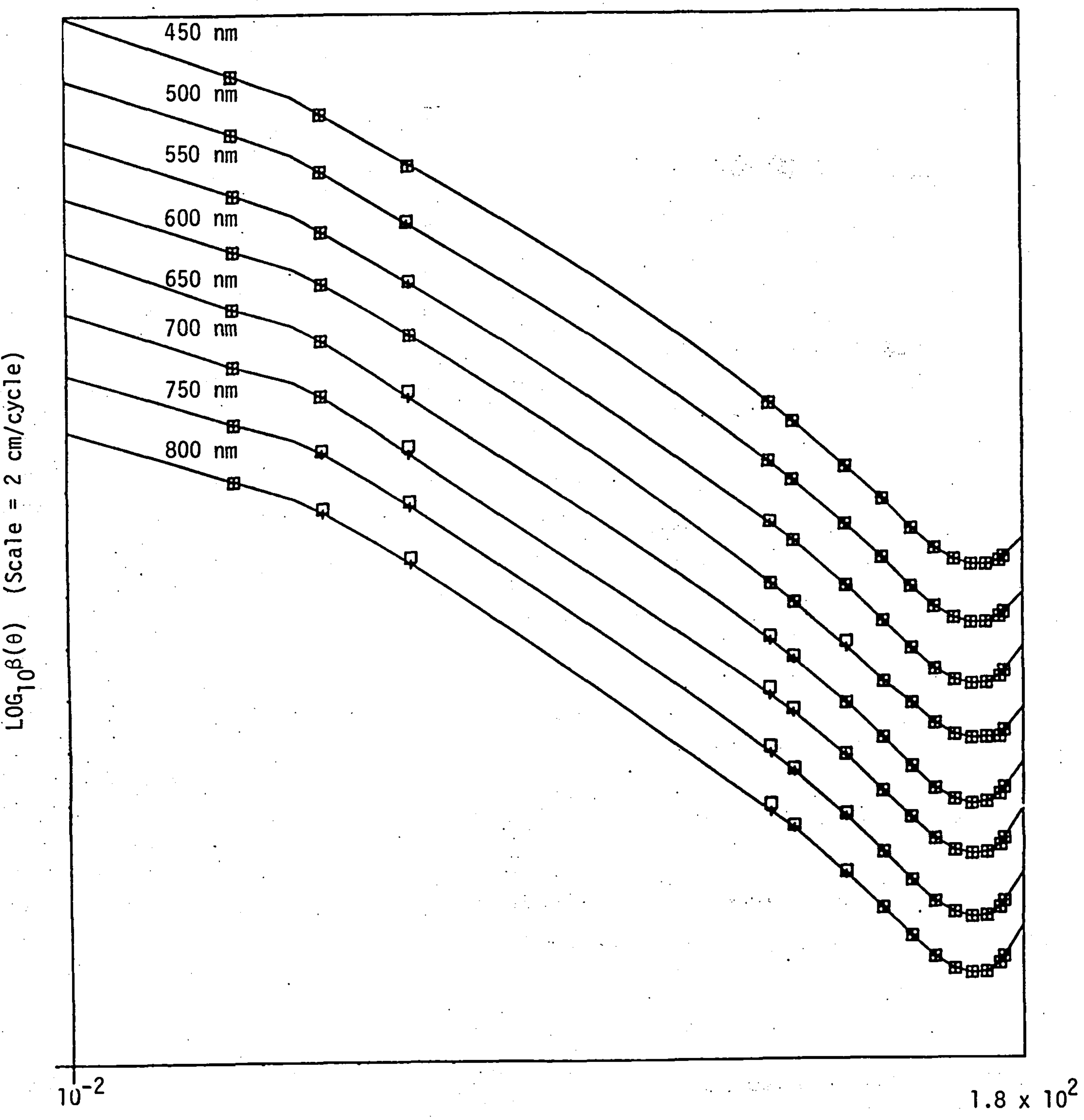

Figure A2. Volume scattering function $\beta(\theta)$ versus scattering angle θ for sample A2. Squares are centered on measured data and crosses on adjusted values.

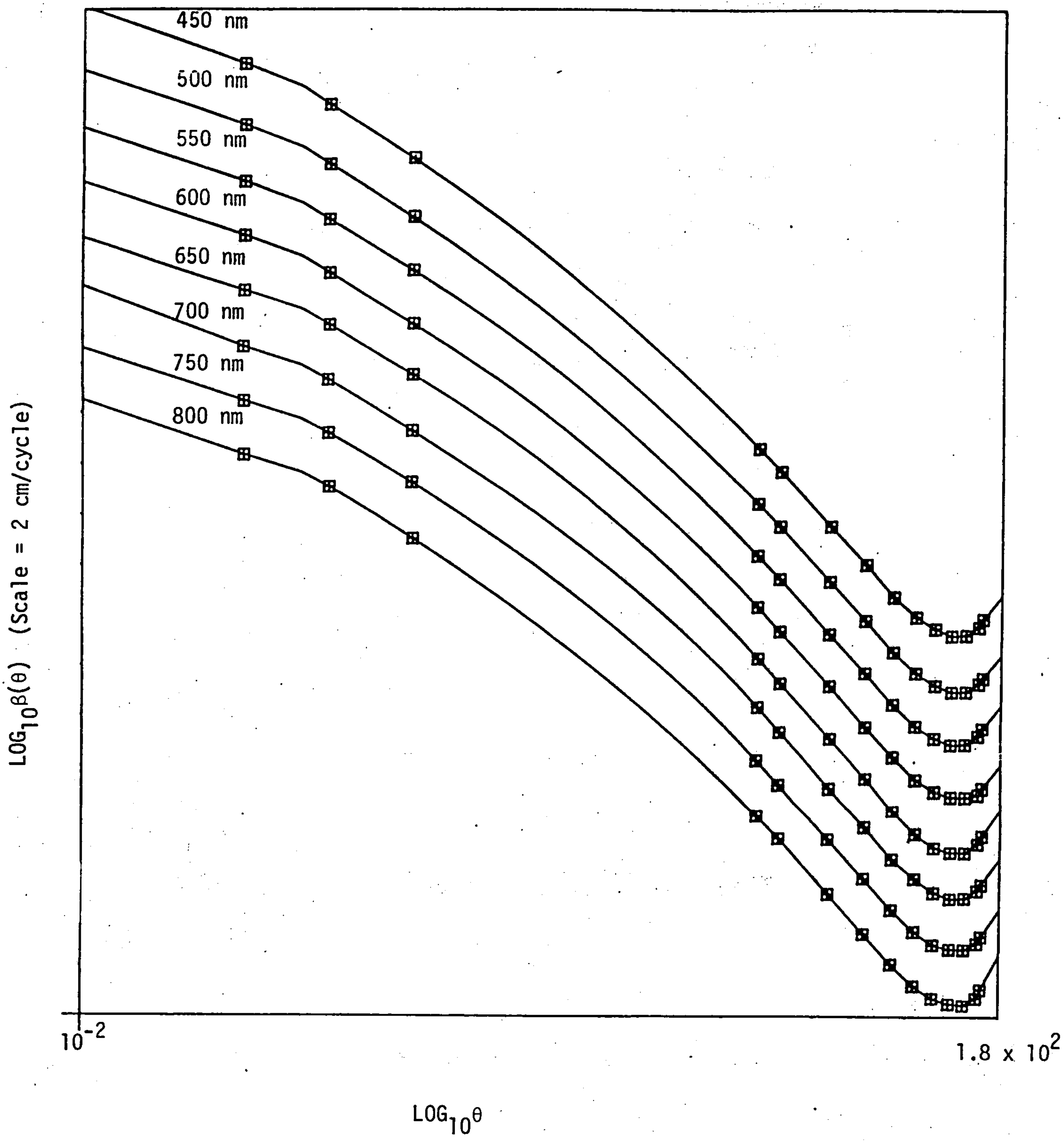

Figure A3. Volume scattering function $\beta(\theta)$ angle θ for sample B. Squares are centered on measured data and crosses on adjusted values

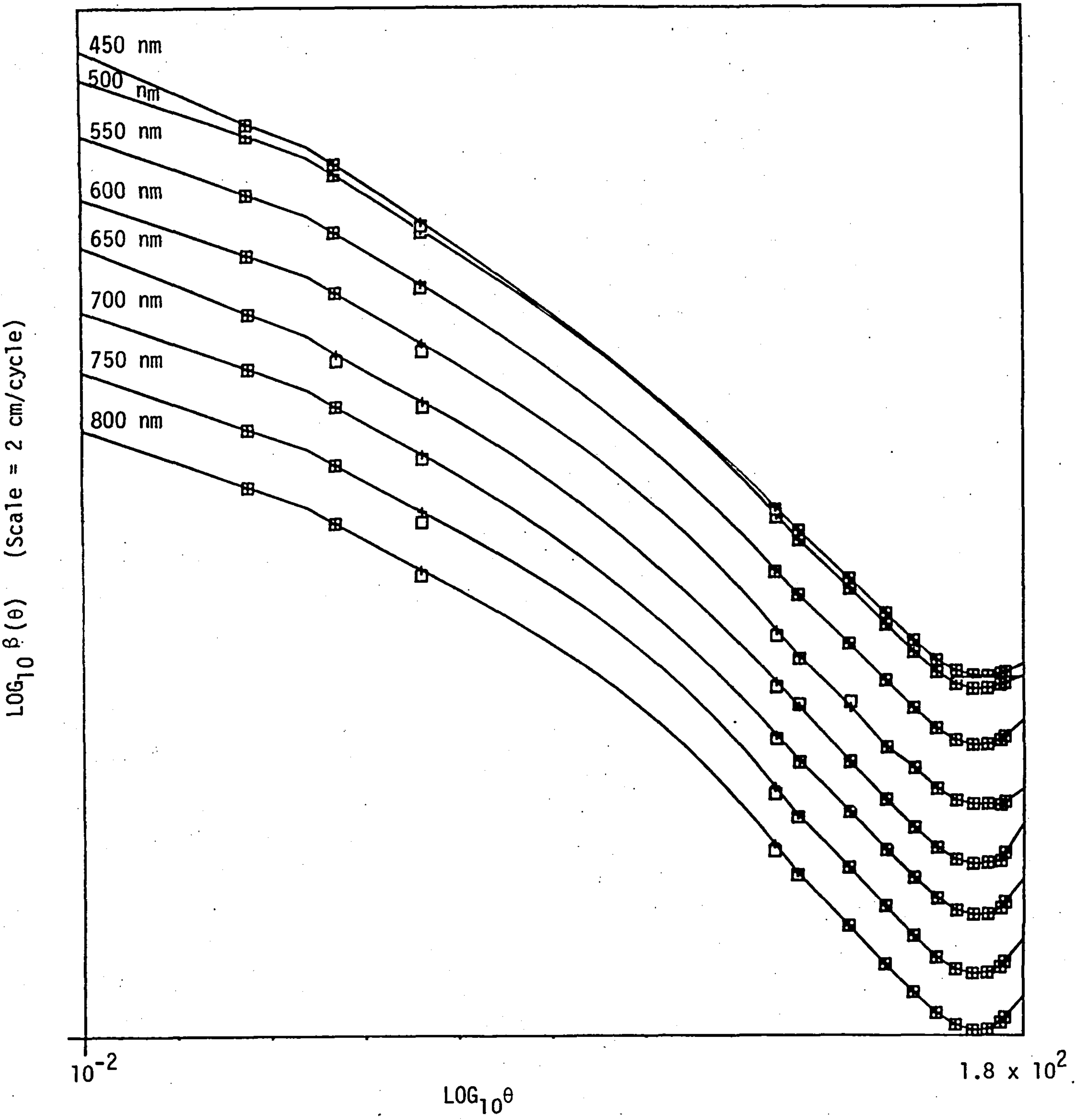

Figure A4. Volume scattering function $\beta(\theta)$ versus scattering angle θ for sample G1. Squares are centered on measured data and crosses on adjusted values.

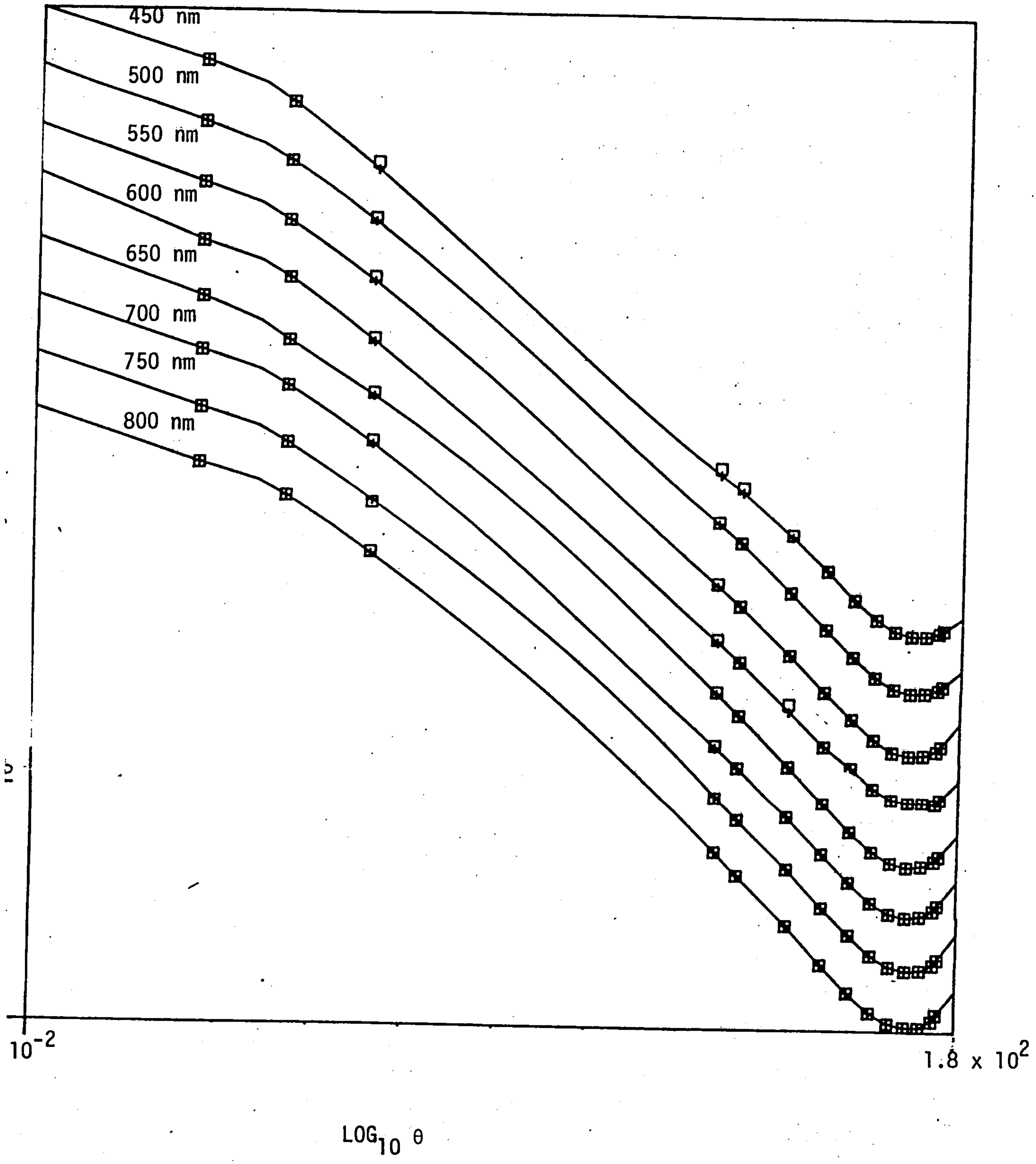

Figure A5. Volume scattering function $\beta(\theta)$ versus scattering angle θ for sample G2. Squares are centered on measured data and crosses on adjusted values.

APPENDIX B

SUPPLEMENTAL MONTE CARLO RESULTS

Figures B1 through B6 provide additional comparisons of Gordon's Power Series results with Monte Carlo simulations versus solar zenith angle and the single scattering albedo.

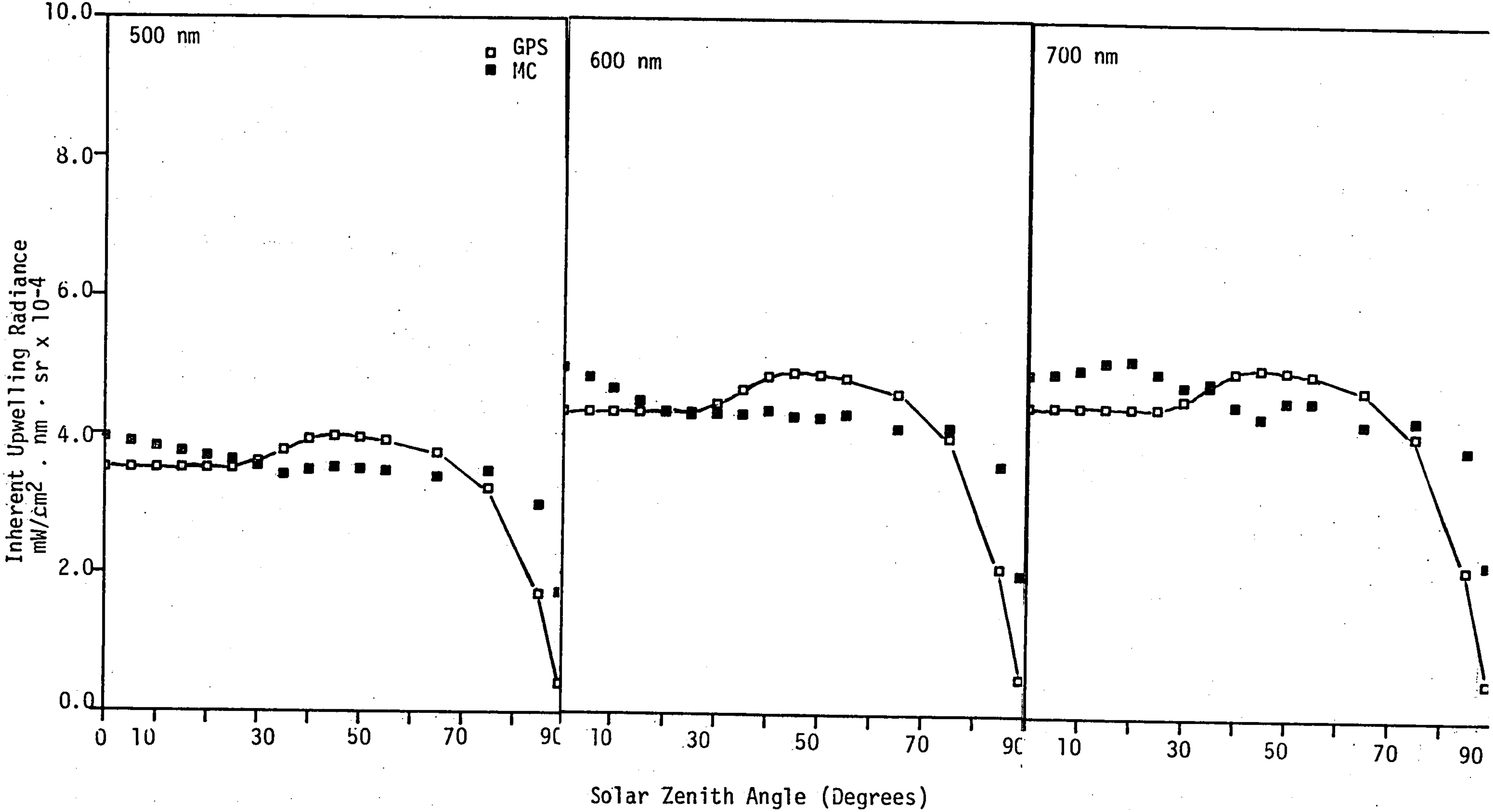

Figure B1. Comparison of Gordon's Power Series Approximation (GPS) with Monte Carlo (MC) Results versus Solar Zenith Angle for Sample A1.

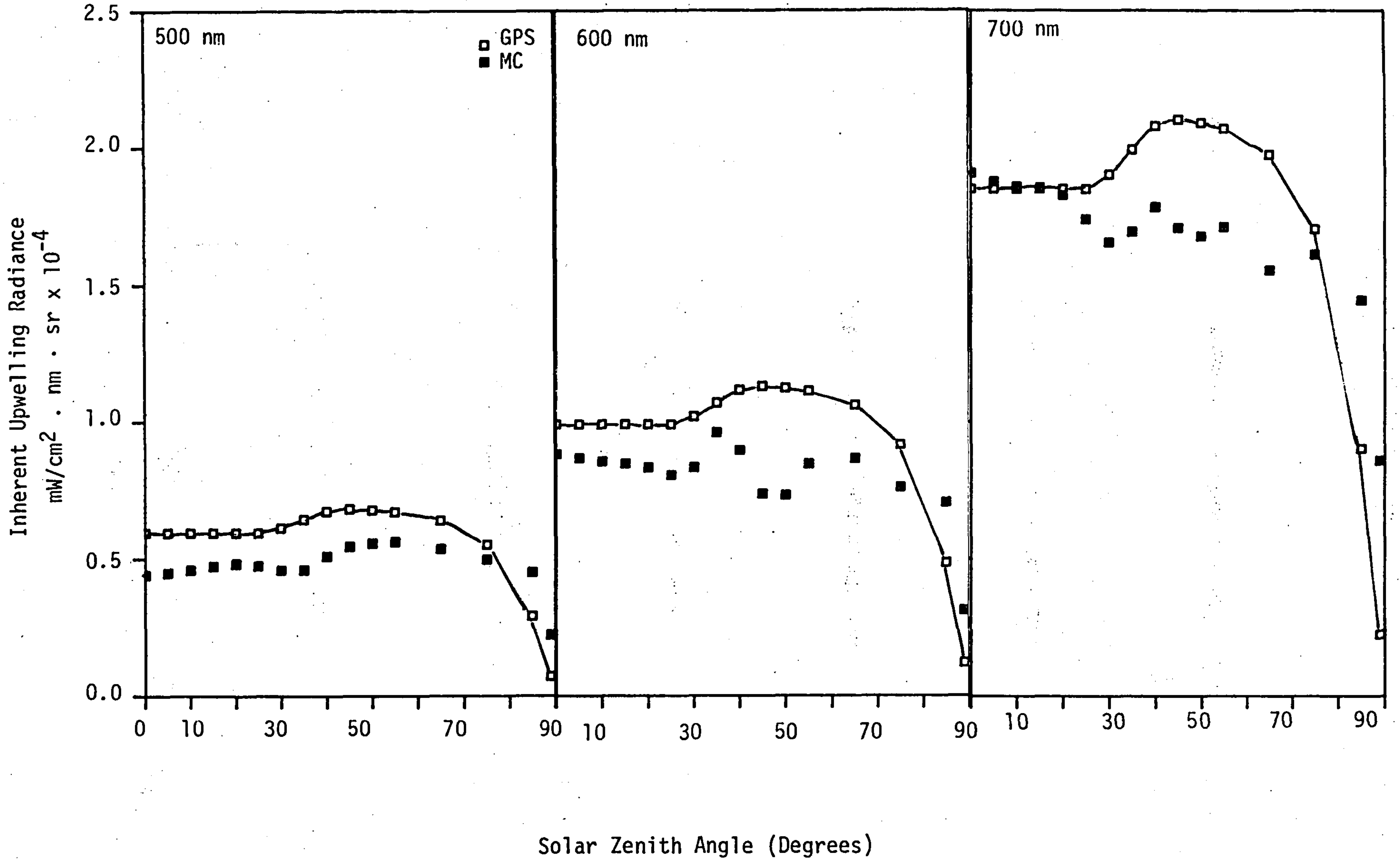

Figure B2. Comparison of Gordon's Power Series Approximation (GPS) with Monte Carlo Results (MC) versus Solar Zenith Angle for Sample G1

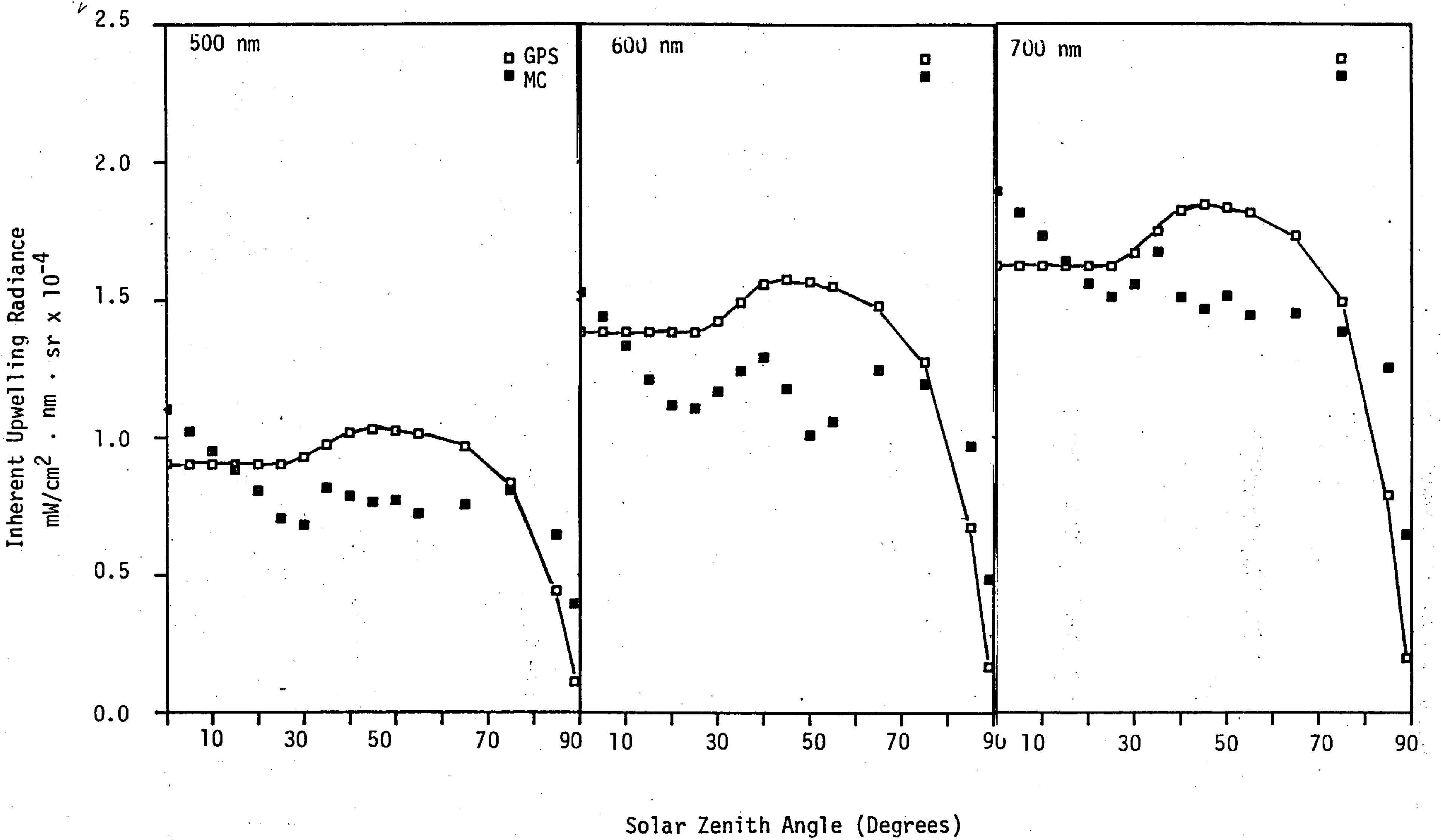

Figure B3. Comparison of Gordon's Power Series Approximation (GPS) with Monte Carlo Results (MC) versus Solar Zenith Angle for Sample G2

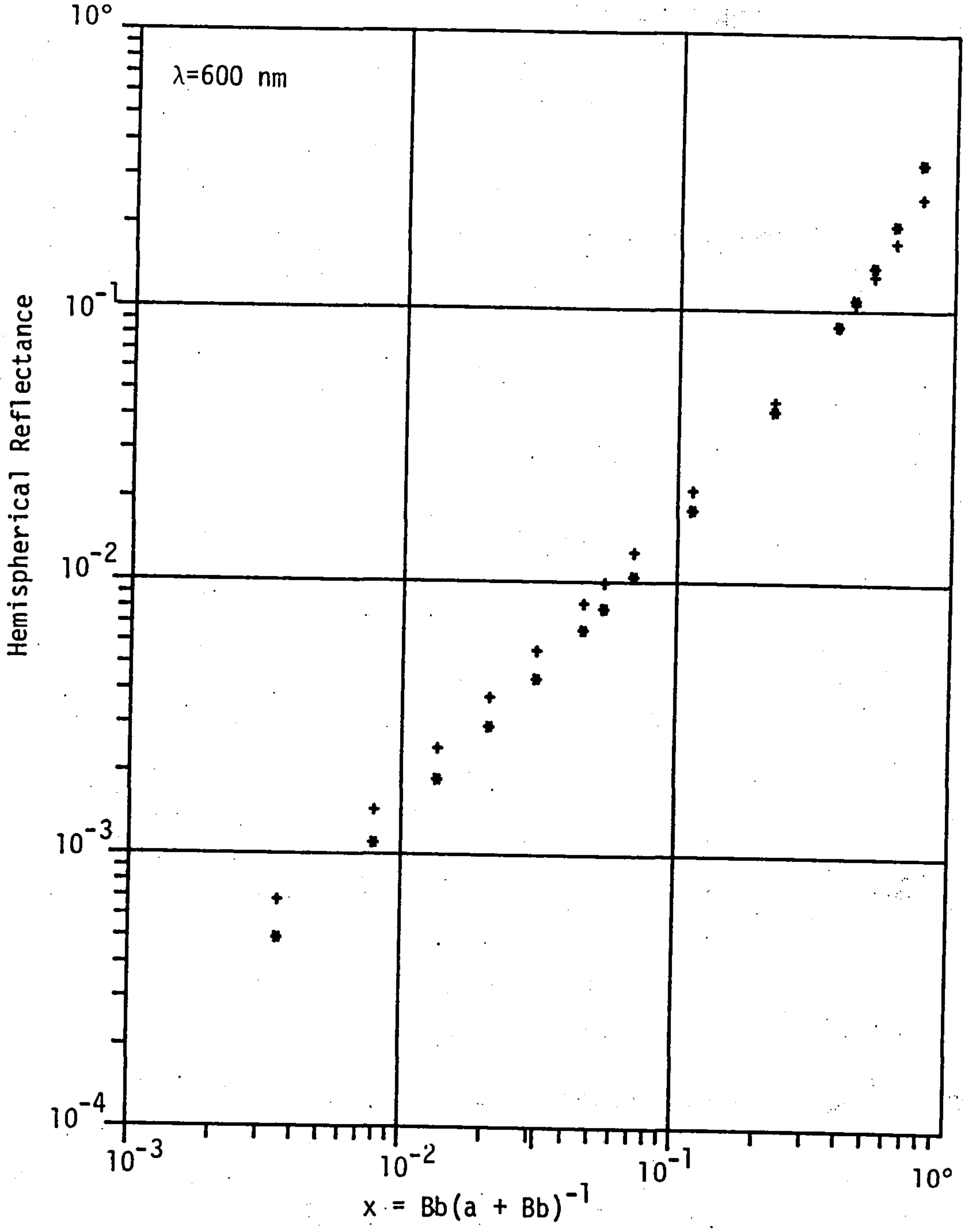

Figure B4. GPS Model (+) and Monte Carlo (*) Predicted Above Surface Hemispherical Reflectance versus $Bb(a + Bb)^{-1}$. Sunlight is direct from Zenith and Sample B Optical Properties were assumed.

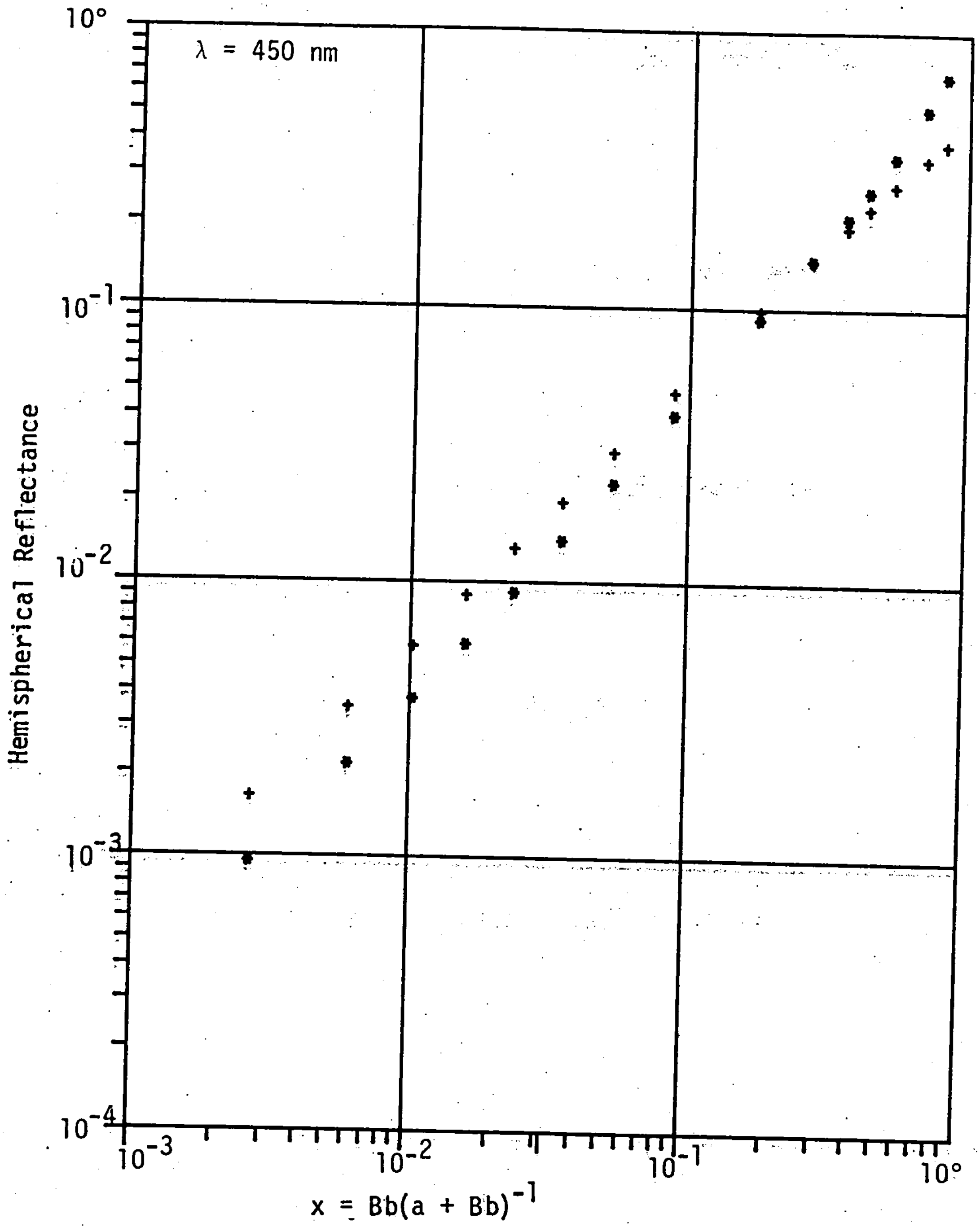

Figure B5. GPS Model (+) and Monte Carlo (*) Predicted Above Surface Hemispherical Reflectance versus $Bb(a + Bb)^{-1}$. Sunlight is Direct from Zenith and Sample A2 Optical Properties were assumed.

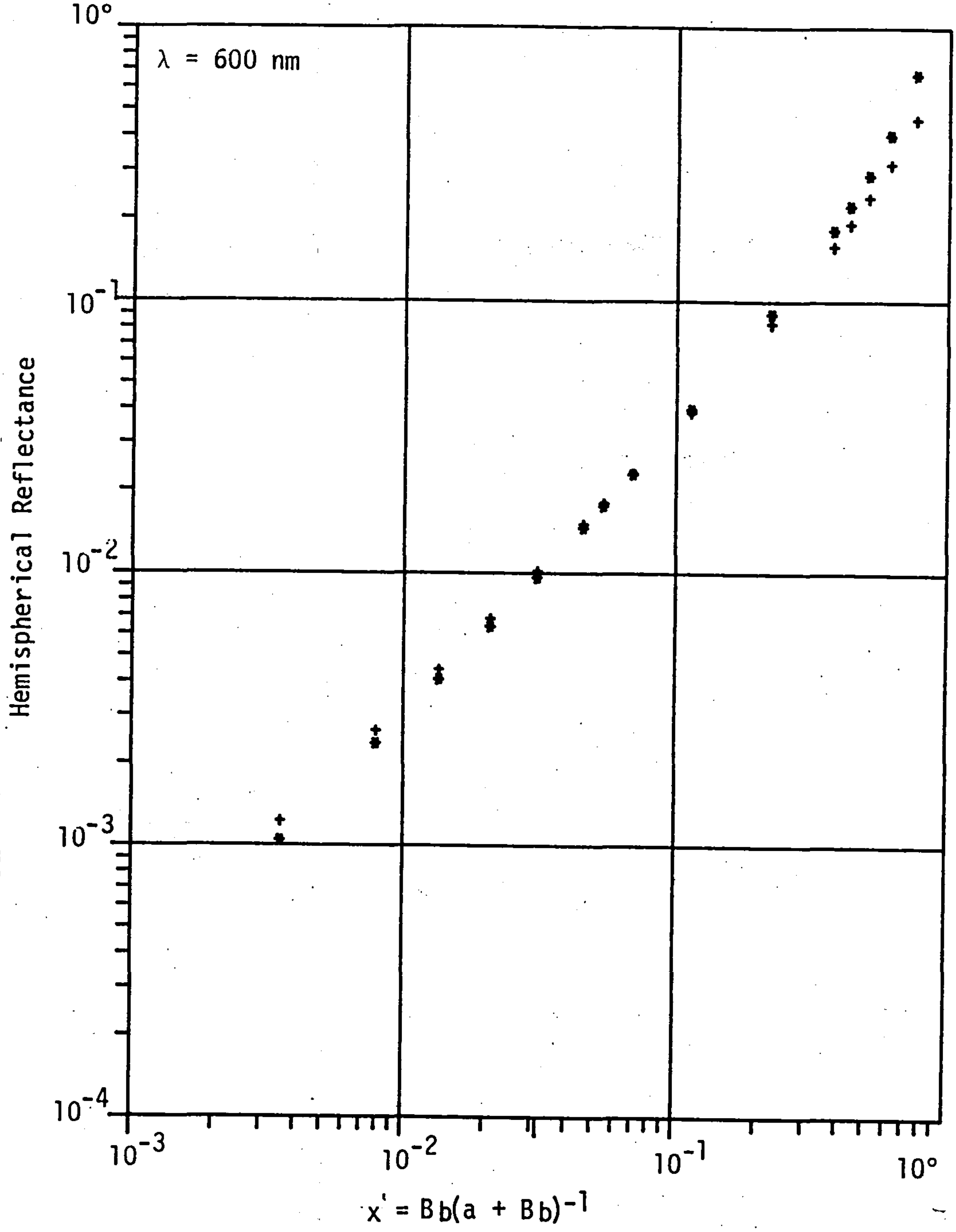

Figure B6. GPS Model (+) and Monte Carlo (*) Predicted Below Surface Hemispherical Reflectance versus $B_b(a + B_b)^{-1}$. Sunlight is direct from zenith and sample G1 optical properties were assumed.

1. Report No. NASA CR-165741	2. Government Accession No.	3. Recipient's Catalog No.

4. Title and Subtitle

VERIFICATION OF REFLECTANCE MODELS IN TURBID WATERS

5. Report Date
April 1981

6. Performing Organization Code

7. Author(s)

Fred J. Tanis and David R. Lyzenga

8. Performing Organization Report No.
137000-39-F

9. Performing Organization Name and Address

Environmental Research Institute of Michigan
Post Office Box 8618
Ann Arbor, Michigan 48107

10. Work Unit No.

11. Contract or Grant No.
NAS1-15512

12. Sponsoring Agency Name and Address
National Aeronautics and Space Administration
Washington, DC 20546

13. Type of Report and Period Covered
Contractor Report

14. Sponsoring Agency Code

15. Supplementary Notes
Langley Technical Monitor - Lamont R. Poole
Alternate - Charles Whitlock
Final Report - August 1978-April 1981

16. Abstract

Field measurements of inherent optical parameters of very turbid waters were used to evaluate existing water reflectance models. Measured upwelling radiance spectra and Monte Carlo simulations of the radiative transfer equations were compared with results from models based upon two flow, quasi-single scattering, augmented isotropic scattering, and power series approximation. Each model was evaluated for three separate components of upwelling radiance (1) direct sunlight, (2) diffuse skylight, and (3) internally reflected light. Limitations of existing water reflectance models as applied to turbid waters are discussed as well as possible applications to the extraction of water constituent information.

17. Key Words (Suggested by Author(s))
Monte Carlo Simulation
Water Reflectance Models
Inherent Optical Properties
Upwelling Radiance Spectra

18. Distribution Statement

Unclassified - Unlimited

Subject Category 43

19. Security Classif. (of this report) Unclassified	20. Security Classif. (of this page) Unclassified	21. No. of Pages 70	22. Price A04

N-305

For sale by the National Technical Information Service, Springfield, Virginia 22161